Celestial Mechanics and Dynamical Astronomy (2022) 134:38
https://doi.org/10.1007/s10569-022-10094-4

ORIGINAL ARTICLE

Recent arrivals to the main asteroid belt

Carlos de la Fuente Marcos[1] · **Raúl de la Fuente Marcos**[2]

Received: 14 November 2021 / Revised: 11 July 2022 / Accepted: 12 July 2022

Abstract
The region where the main asteroid belt is now located may have started empty, to become populated early in the history of the Solar system with material scattered outward by the terrestrial planets and inward by the giant planets. These dynamical pathways toward the main belt may still be active today. Here, we present results from a data mining experiment aimed at singling out present-day members of the main asteroid belt that may have reached the belt during the last few hundred years. Probable newcomers include 2003 BM_1, 2007 RS_{62}, 457175 (2008 GO_{98}), 2010 BG_{18}, 2010 JC_{58}, 2010 JV_{52}, 2010 KS_6, 2010 LD_{74}, 2010 OX_{38}, 2011 QQ_{99}, 2013 HT_{149}, 2015 BH_{103}, 2015 BU_{525}, 2015 RO_{127}, 2015 RS_{139}, 2016 PC_{41}, 2016 UU_{231}, 2020 SA_{75}, 2020 UO_{43}, and 2021 UJ_5, all of them in the outer belt. Some of these candidates may have been inserted in their current orbits after experiencing relatively recent close encounters with Jupiter. We also investigated the likely source regions of such new arrivals. Asteroid 2020 UO_{43}, if real, has a non-negligible probability of having an origin in the Oort cloud or even interstellar space. Asteroid 2003 BM_1 may have come from the neighborhood of Uranus. However, most newcomers—including 457175, 2011 QQ_{99}, and 2021 UJ_5—might have had an origin in Centaur orbital space. The reliability of these findings is assessed within the context of the uncertainties of the available orbit determinations.

Keywords Main belt · Centaurs · Statistical analysis

1 Introduction

Between the orbits of Mars and Jupiter, there is a diverse population of small bodies known collectively as the main asteroid belt (see, for example, the review by Raymond and Nesvorny 2022). Although there is general agreement that the main belt formed early in the history of

This article is part of the topical collection on Main Belt Dynamics
Guest Editors: Christoph Lhotka, Vladislav Sidorenko and Alessandra Celletti.

✉ Carlos de la Fuente Marcos
nbplanet@ucm.es

[1] Universidad Complutense de Madrid, Ciudad Universitaria, 28040 Madrid, Spain

[2] AEGORA Research Group, Facultad de Ciencias Matemáticas, Universidad Complutense de Madrid, Ciudad Universitaria, 28040 Madrid, Spain

Published online: 16 August 2022

the Solar system, the exact details of its origins remain uncertain. Shortly after the discovery of the first members of the main asteroid belt, H. W. M. Olbers and others proposed that these objects could be debris from a destroyed planet (see, for example, the reviews and notes by Bobrovnikoff 1931; Kuiper 1950; Ovenden 1972; Napier and Dodd 1973) or leftover material that never made into a planet due to, namely, collisional processes (see, for example, Kuiper 1950; Alfvén 1964; Napier and Dodd 1974; Petit et al. 2001). However, Raymond and Izidoro (2017) pointed out that dark, water-rich carbonaceous C-type asteroids dominate the outer belt and drier, siliceous S-type asteroids are more common in the inner belt. Such a trend led these authors to propose that the region where the main asteroid belt is now located started empty and that the currently observed asteroids were inserted there from the inner Solar system (S-types) and from the region of the giant planets (C-types). In this scenario, material spread outward by the terrestrial planets contributed to the S-type asteroid population currently inhabiting the main belt; debris scattered inward mainly by Jupiter and Saturn ended up contributing to the C-type component of the belt. The presence in the main asteroid belt of material formed well beyond Jupiter and Saturn has been dramatically confirmed by Hasegawa et al. (2021), who found two extremely red main-belt asteroids, 203 Pompeja and 269 Justitia. Such red bodies may share an origin with trans-Neptunian objects (TNOs) and Centaurs that have surfaces covered with complex organics (see, for example, Barucci et al. 2008). However, red carbonaceous asteroids may turn less red over time because of space weathering (see, for example, Hasegawa et al. 2022).

As the current orbital architecture of the coupled subsystems made of the inner and outer planets may have remained in its present form for Gyr (see, for example, Innanen et al. 1998; Ito and Tanikawa 1999, 2002; Tanikawa and Ito 2007; Mikkola and Lehto 2022), it is reasonable to assume that the dynamical pathways that might have populated the main asteroid belt in the past could still be open today. In order to investigate such a possibility, numerical integrations may be used to identify present-day members of the main asteroid belt that may have followed significantly different orbits in the relatively recent past. There are, however, over 10^6 known main-belt members and a blind search would require a very substantial amount of computer power in order to complete the task. In sharp contrast, a data mining exploration of a reliable database may lead to robust results using just modest resources. Here, we present results from a data mining experiment aimed at singling out present-day members of the main asteroid belt that may have reached the belt during the last few hundred years. In a way, our investigation is the exact opposite of the one discussed by Granvik et al. (2017) that focused on the escape of asteroids from the main belt. This paper is organized as follows. In Sect. 2, we present the data and methods used in our analyses, which are shown in Sect. 3. In Sect. 4, we apply N-body simulations to further study some objects of interest singled out by our statistical analyses. In Sect. 5, we discuss our results. Our conclusions are summarized in Sect. 6.

2 Data and methods

As of April 22, 2022, the Minor Planet Center (MPC)[1] had 344.0 million of observations of 1,194,113 asteroids and 4405 comets (see, for example, Rudenko 2015, 2016; Hernandez et al. 2019). The vast majority of the data corresponded to members of the main asteroid belt. The data are available from the MPC itself and, in somewhat processed form, from several

[1] https://minorplanetcenter.net/

other online resources that include the Jet Propulsion Laboratory (JPL)[2]-hosted ensemble of small-bodies websites and the European Asteroids Dynamic Site (ASTDyS)[3] online information service (see, for example, Knezevic and Milani 2012; Bernardi 2015). These databases can be queried using tools available from the websites themselves, but also through several packages written in the `Python` language (Van Rossum and Drake 1995, 2009).

2.1 Data

Here, we work with publicly available data (orbit determinations, input Cartesian vectors, ephemerides) from JPL's Small-Body Database (SBDB)[4] and `Horizons` online solar system data and ephemeris computation service,[5] both provided by the Solar System Dynamics Group (SSDG,[6] Giorgini et al. 1996; Chamberlin et al. 1997; Giorgini et al. 1997; Giorgini 2011, 2015). The `Horizons` ephemeris system has recently been updated, replacing the DE430/431 planetary ephemeris, used since 2013, with the new DE440/441 solution (Park et al. 2021). DE440 covers the years 1550–2650 while DE441 is tuned to cover a time range of −13,200 to +17,191 years (Park et al. 2021). The new DE440/441 general-purpose planetary solution includes seven additional years of ground and space-based astrometric data, data calibrations, and dynamical model improvements, most significantly involving Jupiter, Saturn, Pluto, and the Kuiper Belt (Park et al. 2021). Most data were retrieved from JPL's SBDB and `Horizons` using tools provided by the `Python` package `Astroquery` (Ginsburg et al. 2019) and its `HorizonsClass` class.[7]

2.2 Methods

The statistical analyses in Sect. 3 have been carried out using tools from several `Python` packages (`Python 3.9` and the latest versions of the libraries were used). Some figures have been produced using the `Matplotlib` library (Hunter 2007) and statistical tools provided by `NumPy` (van der Walt et al. 2011; Harris et al. 2020). Sets of bins in frequency-based histograms were computed using `NumPy` by applying the Freedman and Diaconis rule (Freedman and Diaconis 1981).

The N-body simulations discussed in Sect. 4 were carried out using a direct N-body code developed by Aarseth (2003) that is publicly available from the website of the Institute of Astronomy of the University of Cambridge.[8] This software uses the Hermite integration scheme implemented by Makino (1991). This scheme applies a predictor–corrector time integration method that uses an extrapolation of the equations of motion to predict positions and velocities from which the new accelerations are computed; then, the predicted values are corrected using interpolation by applying finite differences techniques. The Hermite scheme allows efficient numerical integration of the entire Solar system thanks to the use of a block-step strategy (Aarseth 2003) in which suitably quantized time-steps allow the precise integration of the orbits of Mercury or planetary satellites and trans-Neptunian objects

[2] https://www.jpl.nasa.gov

[3] https://newton.spacedys.com/astdys/index.php?pc=0

[4] https://ssd.jpl.nasa.gov/tools/sbdb_lookup.html#/

[5] https://ssd.jpl.nasa.gov/horizons/

[6] https://ssd.jpl.nasa.gov/

[7] https://astroquery.readthedocs.io/en/latest/jplhorizons/jplhorizons.html

[8] http://www.ast.cam.ac.uk/~sverre/web/pages/nbody.htm

simultaneously; encounters at very close range can also be followed with sufficient precision (see, for example, the application to the Chelyabinsk event in de la Fuente Marcos et al. 2015). Results from this code have been extensively discussed by de la Fuente Marcos and de la Fuente Marcos (2012) and compare well with those from Laskar et al. (2011) among others. In our calculations, relative errors in the total energy are as low as 10^{-16}–10^{-15}. The relative error in the total angular momentum is several orders of magnitude smaller.

The physical model included gravitational perturbations from the eight major planets, the Moon, the barycentre of the Pluto-Charon system, and the three largest asteroids. When integrating the equations of motion, non-gravitational forces, relativistic or oblateness terms were not taken into account. Besides studying some representative orbits, we performed additional calculations that applied the Monte Carlo using the Covariance Matrix (MCCM) methodology described by de la Fuente Marcos and de la Fuente Marcos (2015) in which a Monte Carlo process generates control or clone orbits based on the nominal orbit but adding random noise on each orbital element by making use of the covariance matrix (that was also retrieved from JPL's SSDG SBDB using the `Python` package `Astroquery` and its `SBDBClass` class).[9]

3 Statistical analysis

In order to identify present-day members of the main belt that may have had very different orbits in the relatively recent past (∼400 yr ago), we retrieved (from JPL's `Horizons` via the `astroquery.jplhorizons` package pointed out above) the heliocentric osculating orbital elements of each known member of the main belt for two epochs (t and t_0): 2459600.5 JD TDB (2022-Jan-21.0 00:00:00.0 TDB, Barycentric Dynamical Time, J2000.0 ecliptic and equinox) and 2305427.5 JD TDB (= A.D. 1599-Dec-12 00:00:00.0 TDB). Then, we computed the absolute relative variation of the value of the orbital elements semimajor axis, eccentricity, and inclination (a, e and i, respectively), Δ_a, Δ_e and Δ_i. For example, $\Delta_a = |a_t - a_{t_0}|/a_t$ gives the absolute relative variation in the value of the semimajor axis. By computing the distributions of Δ_a, Δ_e and Δ_i, we can single out known members of the main belt that had statistically significant different orbits in the recent past. The orbital evolution of such objects can be studied in further detail using N-body simulations to find out about their past dynamical history and most probable origin.

3.1 Inner main belt

Following JPL's SBDB, inner main-belt asteroids have $a < 2.0$ au and $q > 1.666$ au. The current tally of this orbit class is 26,027 objects (as of April 22, 2022). Most objects in this region are Hungaria asteroids that populate the 5:1 mean motion resonance with Jupiter between 1.78 au and 2 au from the Sun (see, for example, Milani et al. 2010).

Figure 1 shows the resulting distributions of the absolute relative variation in the value of the orbital elements semimajor axis, eccentricity, and inclination: Δ_a, Δ_e and Δ_i. We use the 1st and 99th percentiles of the distribution to identify severe outliers (see, for example, Wall and Jenkins 2012). Objects in the 1st percentile of the distribution, particularly in the case of Δ_a, can be considered as unusually dynamically stable; minor bodies in the 99th percentile are the least stable of the sample set and any newcomers to the main belt are expected to be above the 99th percentile of the distribution in Δ_a. In the figure, median values are shown as vertical

[9] https://astroquery.readthedocs.io/en/latest/jplsbdb/jplsbdb.html

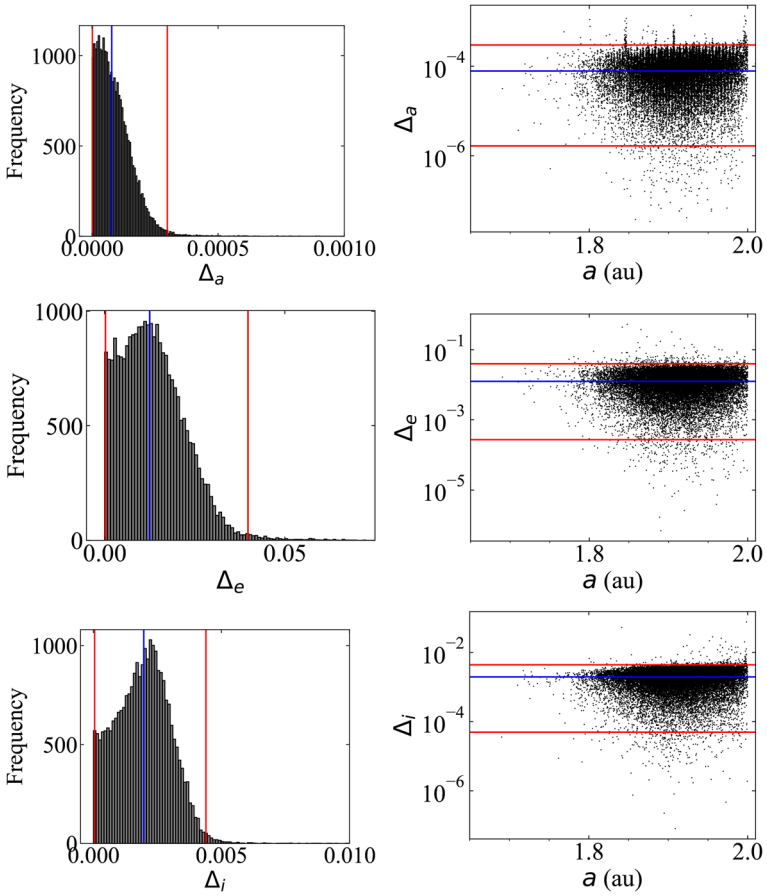

Fig. 1 Inner main belt (26,027 objects as of April 22, 2022). Absolute relative variation in the value of the orbital elements semimajor axis, eccentricity, and inclination: Δ_a, Δ_e and Δ_i. The left-hand side column of panels shows the distributions as frequency histograms; the right-hand side column of panels shows the distribution of absolute relative variations as a function of the semimajor axis in logarithmic scale. Median values are shown as vertical or horizontal blue lines and the 1st and 99th percentiles as red lines. Data source: JPL's `Horizons`

or horizontal blue lines and the 1st and 99th percentiles are displayed as red lines. For Δ_a the 1st, 16th, 50th, 84th, 99th percentiles are: 1.66×10^{-6}, 2.46×10^{-5}, 7.83×10^{-5}, 0.00016 and 0.00030. For Δ_e, the same percentiles are: 0.00027, 0.00424, 0.01253, 0.02226, and 0.03979. And for Δ_i: 4.96×10^{-5}, 0.00077, 0.00197, 0.00300, and 0.00440. The distributions are not normal but in a normal distribution a value that is one standard deviation above the mean is equivalent to the 84th percentile and a value that is one standard deviation below the mean is equivalent to the 16th percentile (see, for example, Wall and Jenkins 2012).

Our analysis shows that the most stable objects, those within the 1st percentile of the distributions, tend to occupy the central regions of the inner belt, with $a \sim 1.9$ au. On the other hand, there are no objects with large values (for example, > 1) of the relative variations. In particular, the maximum value of Δ_a is of the order of 0.0015 (see the right-hand side panels in Fig. 1), which means that the largest variation in the semimajor axis over the studied

time interval is well under 1%. The largest variations are observed in Δ_e. Figure 1, right-hand side top panel, shows that the largest variations are linked to mean motion resonances; the banded distribution observed is the result of the overlapping grid of mean motion resonances with Earth and Mars discussed by Gallardo (2006, 2019). The maxima in the distributions of Δ_e and Δ_i are linked to objects subjected to the von Zeipel–Lidov–Kozai mechanism (von Zeipel 1910; Kozai 1962; Lidov 1962; Ito and Ohtsuka 2019) that drives anti-correlated eccentricity–inclination oscillations. The effects of the von Zeipel–Lidov–Kozai mechanism have been well documented not only within the inner main belt (Michel and Thomas 1996) but in other sections of the belt as well (Vinogradova 2017).

3.2 Main belt

Following JPL's SBDB, main belt asteroids have 2.0 au $< a <$ 3.2 au and $q >$ 1.666 au and this orbit class includes 1,073,121 objects. Figure 2, right-hand side top panel, shows the strong Kirkwood gap at 2.5 au due to the 3:1 mean motion resonance with Jupiter, another one at 2.82 au caused by the 5:2 mean motion resonance with Jupiter, and a third one at 2.958 au linked to the 7:3 mean motion resonance with Jupiter (see, for example, Murray and Dermott 1999).

The maximum values of Δ_a, Δ_e and Δ_i are observed for objects with $a >$ 3.0 au. However, the maximum value of Δ_a is under 0.1 (with one exception); therefore, the largest variation over the studied time interval is still below 10%, not high enough to signal objects that may have entered the main belt in the relatively recent past. Although not as clearly as in Fig. 1, right-hand side top panel, Fig. 2, right-hand side top panel, shows an overlapping grid of mean motion resonances. For Δ_a, the 1st, 16th, 50th, 84th, 99th percentiles are: 7.34×10^{-6}, 0.00012, 0.00044, 0.00134 and 0.00677. For Δ_e, the same percentiles are: 0.00028, 0.00449, 0.01827, 0.06437, and 0.31803. And for Δ_i: 0.00030, 0.00482, 0.01593, 0.04076, and 0.17062. These values are higher than their equivalents for the inner main belt. Our analysis reveals that the most stable objects, those within the 1st percentile of the distributions, tend to occupy the regions with 2.0 au $< a <$ 2.5 au, and they could be as stable as their counterparts in the inner belt.

3.3 Outer main belt

Following JPL's SBDB, outer main-belt asteroids have 3.2 au $< a <$ 4.6 au and the current membership of this orbit class includes 36,901 objects. This region hosts the Hildas (see, for example, Ferraz-Mello et al. 1998), a concentration of asteroids trapped in the 3:2 mean motion resonance with Jupiter (between 3.7 au and 4.2 au), the Cybele asteroids (see, for example, Carruba et al. 2015), in the 7:4 mean motion resonance with Jupiter (between 3.27 au and 3.7 au), and the Thule dynamical group (see, for example, Brož and Vokrouhlický 2008) in the 4:3 mean motion resonance with Jupiter (between 4.26 au and 4.3 au). At 3.27 au, we have the Hecuba gap (see, for example, Roig et al. 2002). The dynamical space between the Cybele, Thule, and Hilda asteroidal populations is unstable because of the overlapping of numerous three-body mean motion resonances, the so-called resonance sea discussed by Gallardo (2006).

Figure 3 shows that this region is by far the most perturbed of the main asteroid belt. The values of the absolute relative variations in a, e, and i are significantly higher than in other regions of the belt. For Δ_a the 1st, 16th, 50th, 84th, 99th percentiles are: 5.25×10^{-5}, 0.00084, 0.00353, 0.00960 and 0.03954. For Δ_e, the same percentiles are: 0.00237, 0.04060, 0.15082,

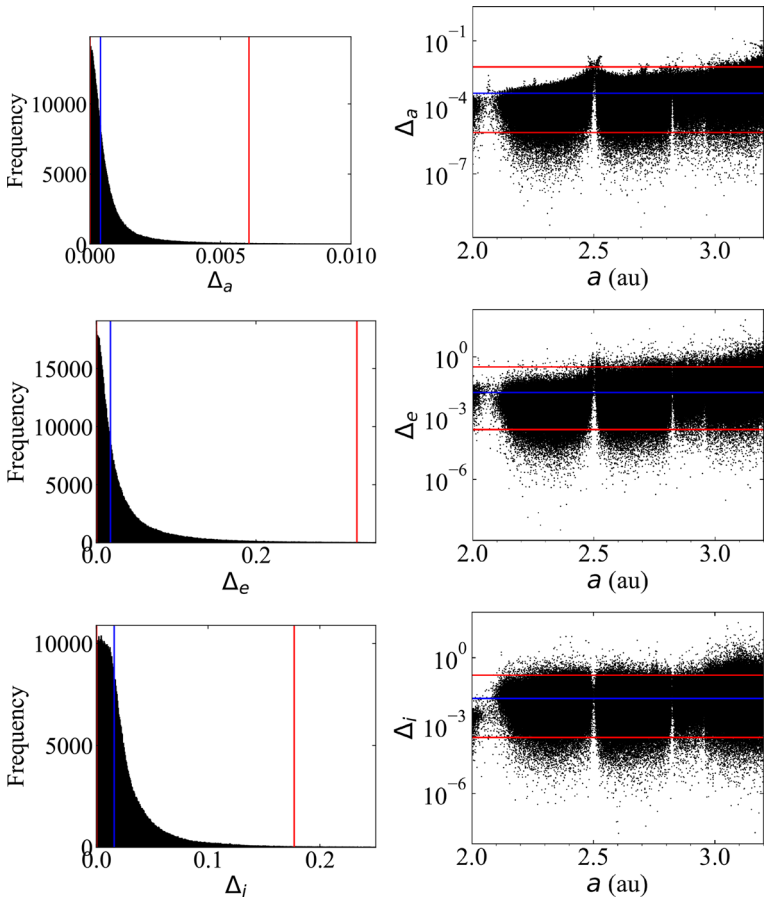

Fig. 2 Main belt's core (1,073,121 objects as of April 22, 2022). Absolute relative variation in the value of the orbital elements semimajor axis, eccentricity, and inclination: Δ_a, Δ_e and Δ_i. The left-hand side column of panels shows the distributions as frequency histograms; the right-hand side column of panels shows the distribution of absolute relative variations as a function of the semimajor axis in logarithmic scale. Median values are shown as vertical or horizontal blue lines and the 1st and 99th percentiles as red lines. Data source: JPL's `Horizons`

0.42004, and 2.13023. And for Δ_i: 0.00035, 0.00586, 0.02082, 0.05824, and 0.45447. Here, we find multiple objects with Δ_a well above the 99th percentile of the distribution. In the following section, we will focus on the subsample with $\Delta_a > 0.6$ that we consider as highly likely to having arrived at the outer main belt in relatively recent times. It is, however, possible that some of such objects are trapped in secular resonances that may bring them back and forth into the belt from beyond Jupiter. If the orbit determinations are robust enough, numerical integrations should be able to confirm their true dynamical nature.

4 Recent arrivals

From the analyses in Sect. 3, we conclude that only the outer main belt hosts a population of minor bodies that may have entered the belt during the last few hundred years. Assuming

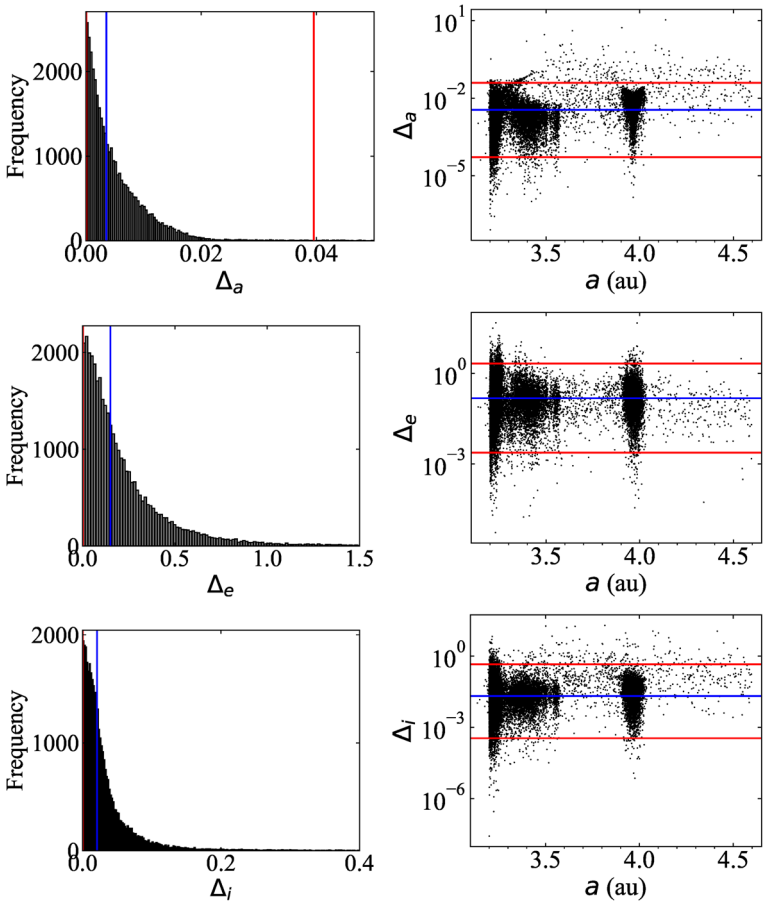

Fig. 3 Outer main belt (36,901 objects as of April 22, 2022). Absolute relative variation in the value of the orbital elements semimajor axis, eccentricity, and inclination: Δ_a, Δ_e and Δ_i. The left-hand side column of panels shows the distributions as frequency histograms; the right-hand side column of panels shows the distribution of absolute relative variations as a function of the semimajor axis in logarithmic scale. Median values are shown as vertical or horizontal blue lines and the 1st and 99th percentiles as red lines. Data source: JPL's `Horizons`

a threshold of $\Delta_a > 0.6$ as pointed out above, the list of recent arrivals in Table 1 includes 2003 BM_1, 2007 RS_{62}, 457175 (2008 GO_{98}), 2010 BG_{18}, 2010 JC_{58}, 2010 JV_{52}, 2010 KS_6, 2010 LD_{74}, 2010 OX_{38}, 2011 QQ_{99}, 2013 HT_{149}, 2015 BH_{103}, 2015 BU_{525}, 2015 RO_{127}, 2015 RS_{139}, 2016 PC_{41}, 2016 UU_{231}, 2020 SA_{75}, 2020 UO_{43}, and 2021 UJ_5.

Unfortunately, most of the objects in Table 1 have very short data arcs and, consistently, their orbit determinations are very uncertain. The objects with the highest probability of being newcomers are 2003 BM_1, 2010 LD_{74}, 2015 BU_{525} and 2020 UO_{43}. Asteroids 2003 BM_1 and 2020 UO_{43} have robust orbit determinations (but see the comment on 2020 UO_{43} later on), but 2010 LD_{74} and 2015 BU_{525} have very poor orbit determinations, based on observational arcs spanning just one day. Minor bodies 2003 BM_1, 2015 BU_{525}, 2020 SA_{75}, 2020 UO_{43}, and 2021 UJ_5 are included in the list of asteroids with comet-like orbits maintained by Y. R.

Table 1 Recent arrivals to the outer main belt (absolute relative variation of the semimajor axis, $\Delta_a > 0.6$).

Object	arc (d)	obs.	a (au)	e	i (^{o})	Δ_a	Δ_e	Δ_i
2003 BM_1	5140	90	3.64009	0.51436	11.34667	4.06475	0.43067	0.28590
2007 RS_{62}	1	9	3.49720	0.36435	0.61698	0.60015	0.97395	1.82065
457175 (2008 GO_{98})	6207	690	3.97017	0.27908	15.55621	0.60318	0.58341	0.03283
2010 BG_{18}	1	11	3.80613	0.25454	17.85287	0.77561	0.12023	0.35398
2010 JC_{58}	2	12	3.63599	0.37660	5.98705	0.73026	0.48396	0.46895
2010 JV_{52}	1	8	3.83195	0.21150	4.12106	1.07049	0.39983	0.74718
2010 KS_6	1	11	3.92736	0.24029	9.39648	0.61127	0.34709	0.29612
2010 LD_{74}	1	15	3.90426	0.32040	18.84908	5.35829	1.50536	0.66081
2010 OX_{38}	1	13	4.11663	0.26317	4.29817	0.81833	0.14387	0.40455
2011 QQ_{99}	8918	48	3.80163	0.42617	3.21247	0.98310	0.30898	3.38391
2013 HT_{149}	2	11	4.15614	0.18113	0.72244	0.66600	0.14155	5.98370
2015 BH_{103}	6	12	4.08323	0.18091	2.04186	0.70796	0.18405	1.07415
2015 BU_{525}	1	17	3.49100	0.51602	8.86846	2.87732	0.38818	0.07012
2015 RO_{127}	3	11	3.57322	0.36363	1.56916	1.12174	0.24970	0.37371
2015 RS_{139}	3	7	4.08529	0.32595	1.35669	1.11238	0.39090	7.32546
2016 PC_{41}	3	11	3.63385	0.39302	8.15787	1.24666	0.14065	0.74684
2016 UU_{231}	1	22	3.57738	0.34396	2.15470	1.04531	0.16766	0.53508
2020 SA_{75}	30	18	3.58730	0.53166	3.03217	1.18201	0.23644	3.66545
2020 UO_{43}	548	13	4.13775	0.64513	1.75827	10.65010	0.72835	1.23496
2021 UJ_5	68	51	3.39604	0.51475	9.38787	1.59925	0.23100	0.65926

The data include number (if assigned by the MPC) and provisional designation, number of days spanned by the data arc, number of observations used to compute the orbit determination, semimajor axis, eccentricity, inclination (these three referred to epoch 2459600.5 JD TDB), absolute relative variation in a, e, and i. Data sources: JPL's SBDB and `Horizons`

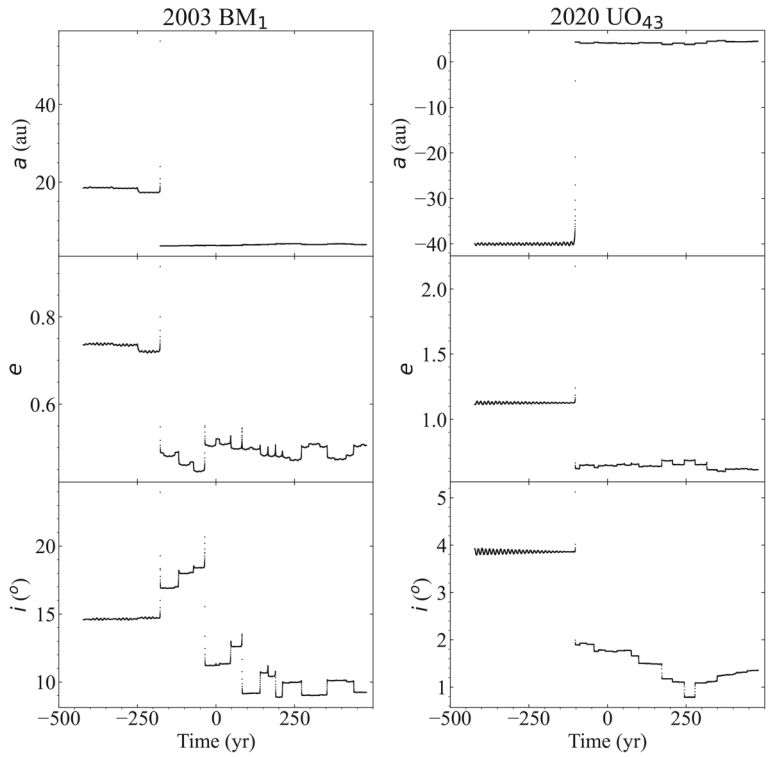

Fig. 4 Evolution of the orbital elements semimajor axis (top panels), eccentricity (middle panels), and inclination (bottom panels) for the nominal orbit of 2003 BM_1 (left-hand side panels) and 2020 UO_{43} (right-hand side panels). For 2020 UO_{43}, the semimajor axis and eccentricity are initially negative and larger than 1, respectively. These values are associated with unbound orbits. The origin of time is the epoch 2459600.5 JD Barycentric Dynamical Time (2022-Jan-21.0 00:00:00.0 TDB) and the output cadence is 30 d. The source of the data is JPL's `Horizons`

Fernández.[10] None of these objects have been studied in detail yet and no cometary activity has ever been observed on any of them.

In sharp contrast and among the rest of the sample, at least one object has been found to exhibit cometary activity, 457175 (2008 GO_{98}), and it has a dual designation as comet 362P (García-Migani and Gil-Hutton 2018; Borysenko et al. 2019; Kokhirova et al. 2021). From this group, only 457175, 2011 QQ_{99}, and 2021 UJ_5 (data arc of 68 d with 51 observations) have robust orbit determinations. It is rather suspicious that out of 15 objects in Table 1 with $0.6 < \Delta_a < 2$ just 20% have sufficiently good orbit determinations, with 80% having very short data arcs, mostly $\leq$3 d. The lack of recovery observations suggests that some of these objects may have been in outburst when discovered and their apparent magnitudes outside their active phases may be too low to enable casual recovery by non-targeted surveys such as those looking for TNOs or near-Earth objects (NEOs). A recent example of an object serendipitously discovered when in the active phase is Centaur 2020 MK_4 (de la Fuente Marcos et al. 2021).

Figure 4 shows the short-term past and future dynamical evolution of the nominal orbits of 2003 BM_1 and 2020 UO_{43} as computed by JPL's `Horizons` (the ephemerides were retrieved

[10] https://physics.ucf.edu/~yfernandez/lowtj.html

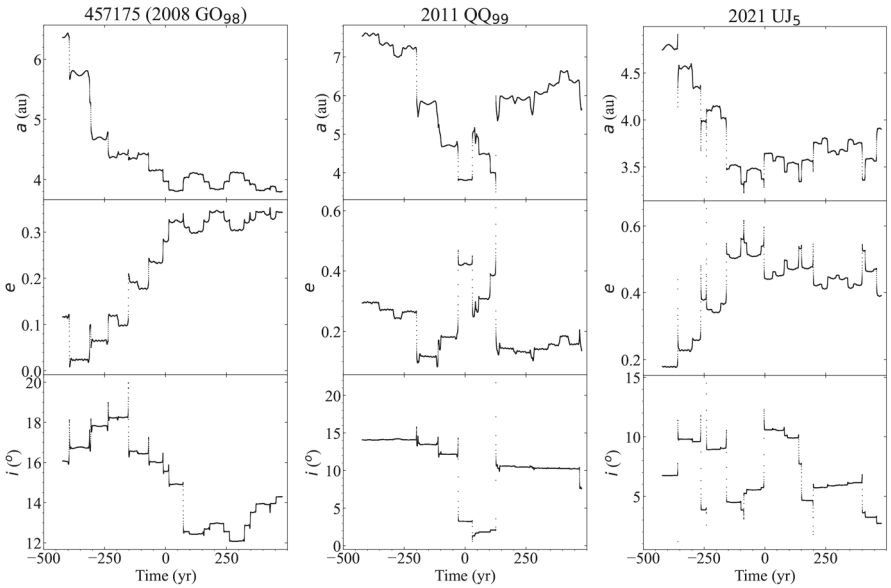

Fig. 5 Evolution of the orbital elements semimajor axis (top panels), eccentricity (middle panels), and inclination (bottom panels) for the nominal orbit of 457175 (2008 GO_{98}), left-hand side panels, 2011 QQ_{99}, central panels, and 2021 UJ_5, right-hand side panels. The origin of time is the epoch 2459600.5 JD Barycentric Dynamical Time (2022-Jan-21.0 00:00:00.0 TDB) and the output cadence is 30 d. The source of the data is JPL's `Horizons`

using the `Astroquery` package as pointed out above and plotted using `Matplotlib`). The two objects exhibit a rather chaotic evolution both in the recent past and into the immediate future. This is the result of planetary encounters at close range (mainly with Jupiter and Saturn, see below). Figure 4, left-hand side top panel, shows that 2003 BM_1 came from the neighborhood of Uranus and arrived at its present location nearly 235 yr ago. However, the most striking case involves 2020 UO_{43} that may have reached its current orbit coming from interstellar space. This object may have entered the Solar system nearly a century ago with an eccentricity of 1.1150, not too different from that of 1I/2017 U1 ('Oumuamua), 1.20113±0.00002, the first known interstellar body passing through the Solar system (see, for example, de la Fuente Marcos and de la Fuente Marcos 2017a, b; Hainaut et al. 2018; Micheli et al. 2018; 'Oumuamua ISSI Team et al. 2019; Seligman et al. 2019).

The second group of newcomers, those with $\Delta_a < 2$, may have come from Centaur orbital space (see, for example, Di Sisto and Brunini 2007; Bailey and Malhotra 2009; Jewitt 2009; Wong et al. 2019; Di Sisto and Rossignoli 2020; Roberts and Muñoz-Gutiérrez 2021). Figure 5 shows the short-term past and future evolution of the three objects with the best orbit determinations of the sample: 457175, 2011 QQ_{99}, and 2021 UJ_5. The three objects have chaotic dynamical histories, but 457175 appears to have followed a one-way path into the outer main belt; the other two objects seem to spend as much time inside the belt as outside of it and even beyond Jupiter's orbit (2011 QQ_{99}). The evolution of the relevant orbital elements of the remaining objects in Table 1 is shown in Fig. 14 of Appendix C. As in the previous case, the jumps in the values of the orbital parameters are the result of planetary encounters at close range (mainly with Jupiter and Saturn, see below).

In the following, we will study in more detail the past dynamical evolution of some of these objects. We will leave outside of our analyses those objects with short data arcs in Table 1 and 457175 because its orbital evolution is affected by the non-gravitational force caused by outgassing. The orbit determination of 457175 available from JPL's SBDB includes the usual orbital elements—a, e, i, longitude of the ascending node, Ω, argument of perihelion, ω, and time of perihelion passage, τ— and three non-gravitational parameters associated with the non-gravitational radial, transverse, and normal accelerations.

4.1 2003 BM_1

This object was first observed on January 24, 2003 by the Near-Earth Asteroid Tracking (NEAT, Helin et al. 1997; Pravdo et al. 1999) program at Palomar Mountain (Lopez et al. 2003). Its orbit determination is based on 90 observations with a data-arc span of 5140 d (see Table 2 in Appendix A). Asteroid 2003 BM_1 follows a rather eccentric path that approaches Mars, but it does not cross its orbit, reaching aphelion beyond Jupiter, which is the only planet that can directly perturb its trajectory. The value of its semimajor axis, 3.64 au, places it in the orbital realm of the Cybele asteroids, but it is not one of them. Figure 4, left-hand side panels, shows that the nominal orbit led 2003 BM_1 into the outer belt from the neighborhood of Uranus. Díaz and Gil-Hutton (2008) included this object in their study of asteroids in cometary orbits concluding that some of those objects are not dormant comet candidates from the Jupiter family—those with Tisserand's parameter, $T_{\rm J}$ (Murray and Dermott 1999), in the range 2–3 and orbital periods under 20 yr or 200 yr, depending on the authors—but asteroids that reached their current orbits as a result of perturbations. The Tisserand parameter, which is a quasi-invariant, is given by the expression:

$$T_{\rm J} = \frac{a_{\rm J}}{a} + 2\,\cos i\,\sqrt{\frac{a}{a_{\rm J}}\,(1-e^2)}\,, \tag{1}$$

where a, e, and i are the semimajor axis, eccentricity and inclination of the orbit of the small body under study, and $a_{\rm J}$ is the semimajor axis of the orbit of Jupiter (Murray and Dermott 1999).

Figure 6 shows the results of N-body integrations backward in time for the nominal orbit and representative control or clone orbits of 2003 BM_1 with Cartesian vectors separated $+3\sigma$ (in green), -3σ (in lime), $+6\sigma$ (in blue), -6σ (in cyan), $+9\sigma$ (in red), and -9σ (in pink) from the nominal values in Table 7 of Appendix B. These calculations have been carried out as described in Sect. 2. Our results are indicative of a very chaotic dynamical past driven by very frequent encounters with Jupiter but also with Saturn, inside the Hill radii of both planets. The evolution is so unstable that some control orbits in Fig. 6 led to ejections from the Solar system (-6σ control orbit in cyan and $+9\sigma$ in red); in other words, 2003 BM_1 has a small probability of having an origin in the Oort cloud and perhaps even in interstellar space. However, our calculations suggest that its most probable source is in the region between the orbits of Jupiter and Neptune, the Centaur orbital domain. The -9σ control orbit (in pink) shows a capture in a von Zeipel–Lidov–Kozai secular resonance with anti-correlated eccentricity–inclination oscillations.

4.2 2020 UO_{43}

This object was first observed on October 20, 2020, by the Pan-STARRS 1 (Kaiser 2004) telescope system at Haleakala. Its orbit determination is based on 13 observations with a

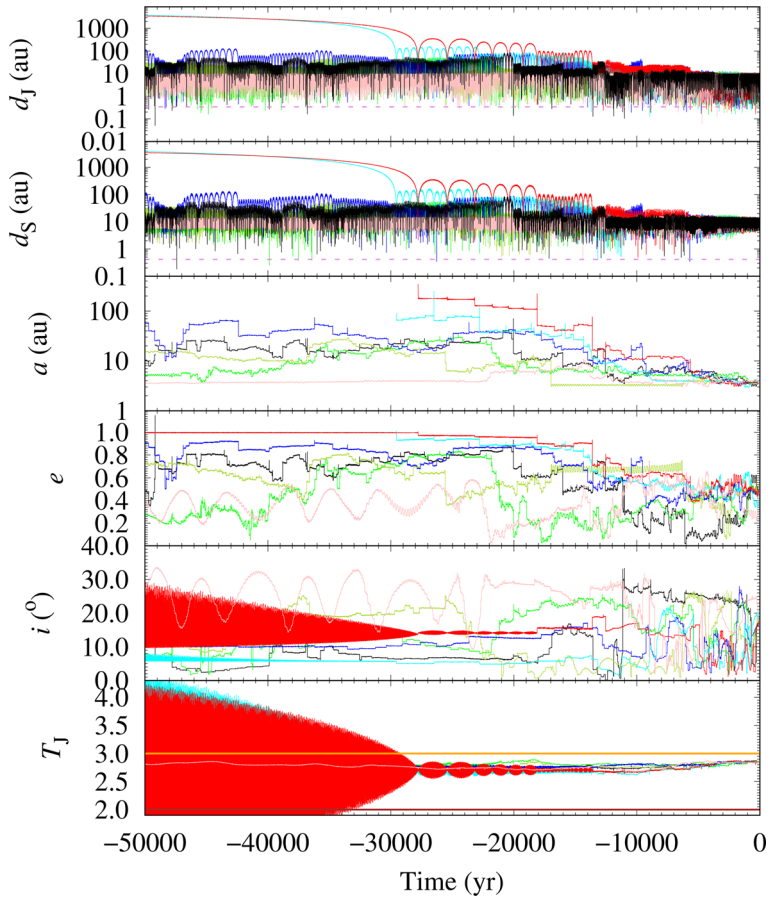

Fig. 6 Short-term past evolution of relevant parameters of 2003 BM_1. We show the evolution of the distance to Jupiter (top panel) and Saturn (second to top) of the nominal orbit (in black) as described by the corresponding orbit determination in Table 2 of Appendix A and those of control orbits or clones with Cartesian vectors separated $+3\sigma$ (in green), -3σ (in lime), $+6\sigma$ (in blue), -6σ (in cyan), $+9\sigma$ (in red), and -9σ (in pink) from the nominal values in Table 7 of Appendix B. The Hill radii of Jupiter, 0.338 au, and Saturn, 0.412 au, are shown in red.The third to top panel shows the evolution of the semimajor axis, a. The third to bottom panel shows the evolution of the eccentricity, e. The second to bottom panel displays the inclination, i. The bottom panel shows the variations in the Tisserand's parameter, T_J (Murray and Dermott 1999), and includes the boundary references 2 (in brown) and 3 (in orange). The output time-step size is 1 yr, the origin of time is epoch 2459600.5 TDB. The source of the input data is JPL's `Horizons`

data-arc span of 548 d (see Table 3 in Appendix A). Asteroid 2020 UO_{43} follows a quite eccentric orbit that crosses that of Mars, reaching aphelion well beyond Jupiter. The value of its semimajor axis, 4.14 au places it within the orbital realm of the Hilda asteroids, but it is not one of them. Figure 4, right-hand side panels, shows that the nominal orbit brought 2020 UO_{43} from interstellar space into the outer belt.

To understand its possible origin better, we performed integrations backward in time using MCCM to generate control orbits and found that the probability of having this object captured from interstellar space during the last 10^5 yr is 0.28 ± 0.05 (average and standard deviation of 8×10^3 experiments). Figure 7 shows the results of these simulations. Most control orbits

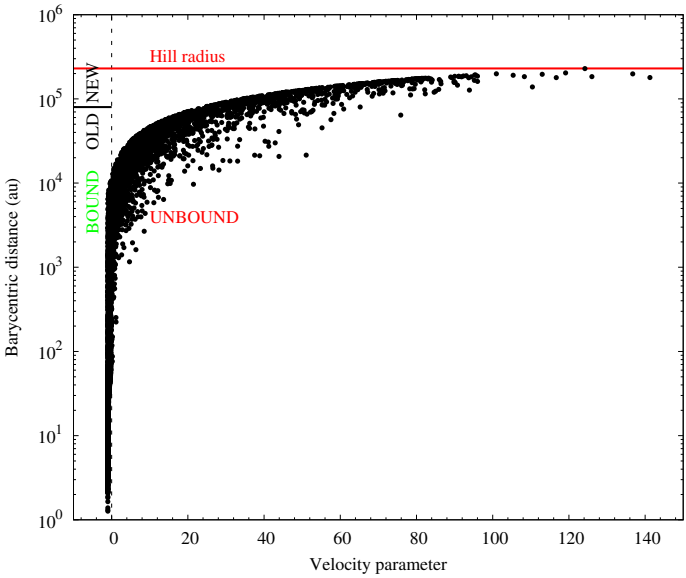

Fig. 7 Values of the barycentric distance as a function of the velocity parameter 10^5 yr into the past for 8×10^3 control orbits of 2020 UO_{43} generated using the MCCM approach. The velocity parameter is the difference between the barycentric and escape velocities at the computed barycentric distance in units of the escape velocity. Positive values of the velocity parameter are associated with control orbits that could be the result of capture. The thick black line corresponds to the aphelion distance—$a\ (1 + e)$, limiting case $e = 1$— that defines the domain of dynamically old comets with $a^{-1} > 2.5 \times 10^{-5}$ au^{-1} (see Królikowska and Dybczyński 2017); the thick red line signals the radius of the Hill sphere of the Solar system (see, for example, Chebotarev 1965)

led to barycentric distances with values below the aphelion distance that defines the domain of dynamically old Oort cloud comets (see Królikowska and Dybczyński 2017). The most straightforward interpretation of these results is that 2020 UO_{43} may have not arrived from interstellar space: It could be a dynamically old object instead, with a likely origin in the Solar system. However, an origin outside the Solar system cannot be rejected with the current orbit determination. In fact, this object might not be real but the result of bad linkage by the MPC.[11]

4.3 210718 (2000 ST_{252})

Asteroid 210718 (2000 ST_{252}) is not in Table 1, but it is included here because it experienced a short-term excursion well outside the outer asteroid belt within the explored time frame. This object was first observed on September 24, 2000, by the Lincoln Near-Earth Asteroid Research (LINEAR) project (Stokes et al. 2000) from Socorro, New Mexico. Its orbit determination is based on 584 observations with a data-arc span of 7822 d (see Table 4 in Appendix A). Asteroid 210718 follows a moderately eccentric orbit that never gets close to Mars, reaching aphelion inside Jupiter's orbit. The value of its semimajor axis, 3.61 au places it in the orbital realm of the Cybele asteroids, but it is not one of them. Figure 8, shows

[11] The 2019 Catalina Sky Survey observations are of 108761 (2001 OK_{46}); the 2020 observations do not correspond to any known object, but are vague enough to have a meaningless orbit and make it effectively unrecoverable (Deen 2022, private communication).

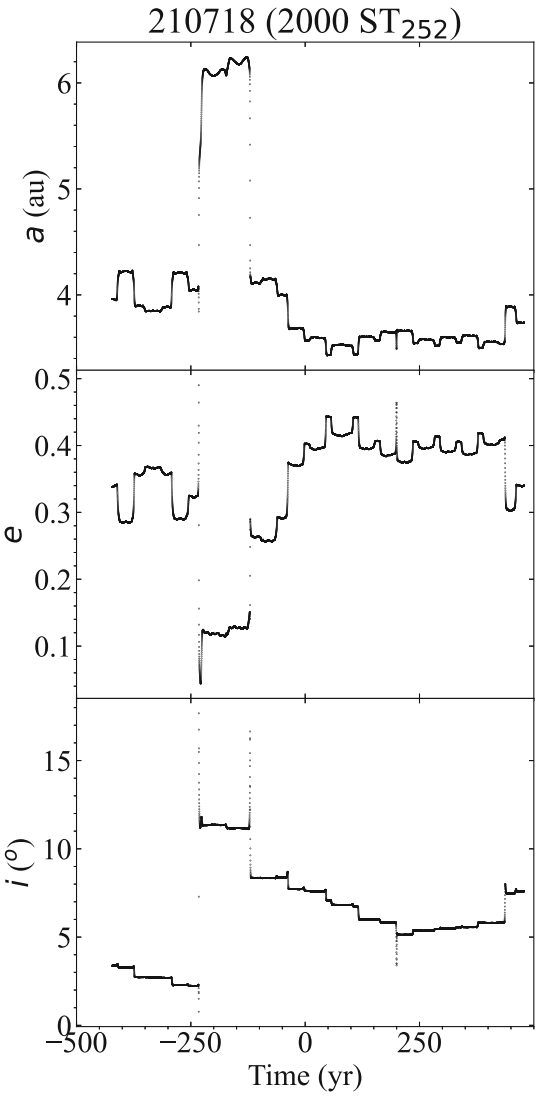

Fig. 8 Evolution of the orbital elements semimajor axis (top panels), eccentricity (middle panels), and inclination (bottom panels) for the nominal orbit of 210718 (2000 ST_{252}) that experiences a short-term excursion well outside the outer asteroid belt within the explored time frame. The origin of time is the epoch 2459600.5 JD Barycentric Dynamical Time (2022-Jan-21.0 00:00:00.0 TDB) and the output cadence is 30 d. The source of the data is JPL's `Horizons`

that the nominal orbit led 210718 into the outer belt from beyond Jupiter, but 400 yr ago it was part of the outer asteroid belt.

Figure 9 shows the result of N-body integrations backward in time for the nominal orbit and representative control orbits of 210718. As in the case of 2003 BM_1, our results show a very chaotic dynamical past driven by frequent encounters with Jupiter and Saturn, inside the Hill radii of both planets. The evolution is quite unstable and one control orbit in Fig. 9 led to an ejection from the Solar system (-6σ control orbit in cyan); therefore, 210718 has a very small probability of having an origin in the Oort cloud and perhaps even in interstellar space. However, our calculations suggest that its most probable source, like in the case of 2003 BM_1, is in the region between the orbits of Jupiter and Neptune, the Centaur orbital domain.

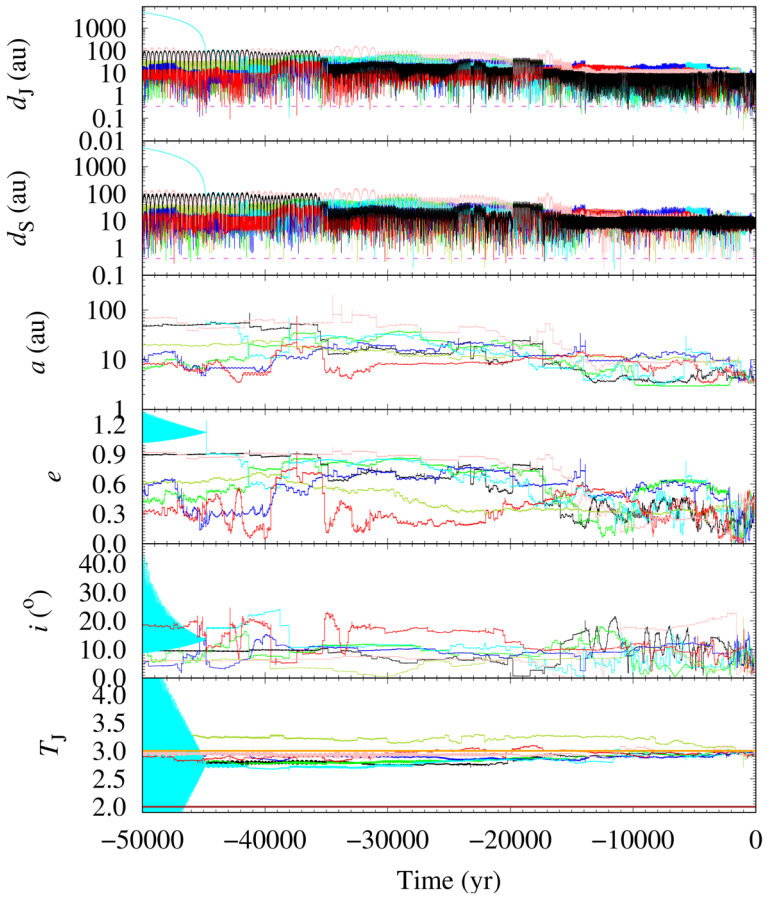

Fig. 9 Short-term past evolution of relevant parameters of 210718 (2000 ST_{252}). We show the evolution of the distance to Jupiter (top panel) and Saturn (second to top) of the nominal orbit (in black) as described by the corresponding orbit determination in Table 4 of Appendix A and those of control orbits or clones with Cartesian vectors separated $+3\sigma$ (in green), -3σ (in lime), $+6\sigma$ (in blue), -6σ (in cyan), $+9\sigma$ (in red), and -9σ (in pink) from the nominal values in Table 8 of Appendix B. The Hill radii of Jupiter, 0.338 au, and Saturn, 0.412 au, are shown in red. The third to top panel shows the evolution of the semimajor axis, a. The third to bottom panel shows the evolution of the eccentricity, e. The second to bottom panel displays the inclination, i. The bottom panel shows the variations in the Tisserand's parameter, T_J (Murray and Dermott 1999), and includes the boundary references 2 (in brown) and 3 (in orange). The output time-step size is 1 yr, the origin of time is epoch 2459600.5 TDB. The source of the input data is JPL's `Horizons`

4.4 2011 QQ_{99}

This object was first observed on September 8, 1996, at the Steward Observatory in Kitt Peak and assigned the provisional designation 1996 RR_{10}. It was rediscovered on August 23, 2011, by the Pan-STARRS 1 (Kaiser 2004) telescope system at Haleakala and assigned the provisional designation 2011 QQ_{99} to being later recognized as the former 1996 RR_{10}. Its orbit determination is based on 48 observations with a data-arc span of 8918 d (see Table 5 in Appendix A). Asteroid 2011 QQ_{99} follows a moderately eccentric orbit that never approaches Mars, reaching aphelion beyond Jupiter that is the only planet that can directly perturb its

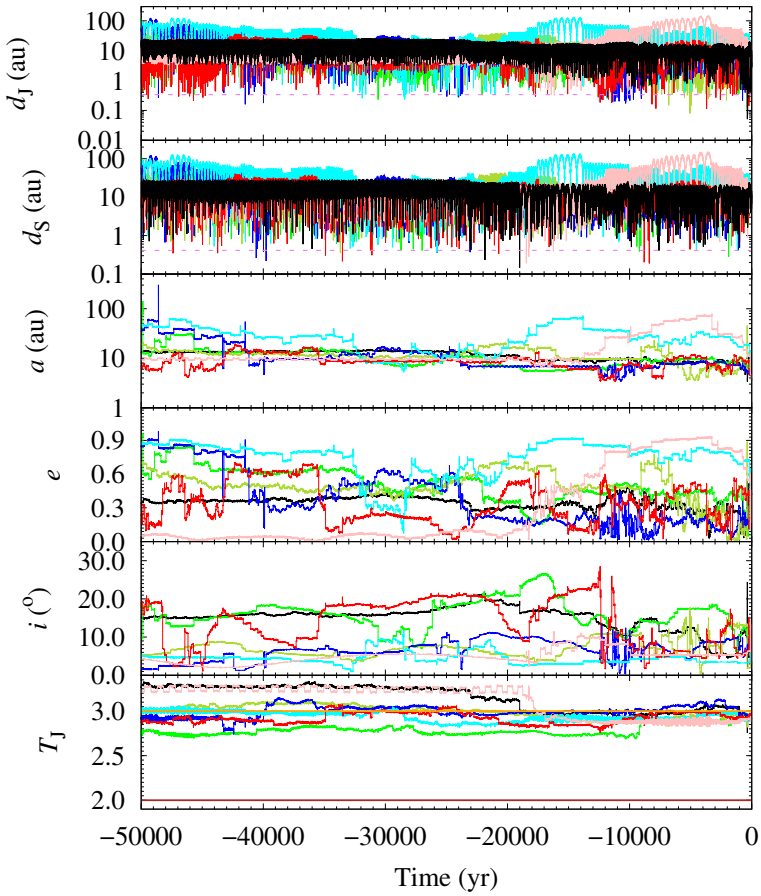

Fig. 10 Short-term past evolution of relevant parameters of 2011 QQ_{99}. We show the evolution of the distance to Jupiter (top panel) and Saturn (second to top) of the nominal orbit (in black) as described by the corresponding orbit determination in Table 5 of Appendix A and those of control orbits or clones with Cartesian vectors separated $+3\sigma$ (in green), -3σ (in lime), $+6\sigma$ (in blue), -6σ (in cyan), $+9\sigma$ (in red), and -9σ (in pink) from the nominal values in Table 9 of Appendix B. The Hill radii of Jupiter, 0.338 au, and Saturn, 0.412 au, are shown in red. The third to top panel shows the evolution of the semimajor axis, a. The third to bottom panel shows the evolution of the eccentricity, e. The second to bottom panel displays the inclination, i. The bottom panel shows the variations in the Tisserand's parameter, T_J (Murray and Dermott 1999), and includes the boundary references 2 (in brown) and 3 (in orange). The output time-step size is 1 yr, the origin of time is epoch 2459600.5 TDB. The source of the input data is JPL's `Horizons`

path. The value of its semimajor axis, 3.80 au places it within the orbital parameter space of the Hilda asteroids, but it is not one of them. Figure 5, second-to-right-hand side panels, shows that the nominal orbit led 2011 QQ_{99} in and out of the outer belt.

Figure 10 shows the result of N-body integrations backward in time for the nominal orbit and representative control orbits of 2011 QQ_{99} (input Cartesian vectors from data in Table 9 of Appendix B). Our results show a very chaotic dynamical past driven again by frequent encounters with Jupiter and Saturn, inside the Hill radii of both planets. The evolution is however somewhat different from those of 210718 or 2003 BM_1. Asteroid 2011 QQ_{99} may remain confined within a relatively narrow volume in orbital parameter space, never venturing

too far from the region of the giant planets. Its source region is probably between the orbits of Jupiter and Neptune, the Centaur orbital domain.

4.5 2021 UJ_5

This object was first observed on October 28, 2021, by the Pan-STARRS 2 (Kaiser 2004) telescope system at Haleakala. Its orbit determination is based on 51 observations with a data-arc span of 68 d (see Table 6 in Appendix A). It has a semimajor axis of 3.40 au, eccentricity of 0.51, and orbital inclination of 9.39°. Its current orbit places it between those of Mars and Jupiter. It may have been a member of the Jupiter-family of comets (Gkotsinas et al. 2022) or related populations such as the comet 29P/Schwassmann-Wachmann 1 or 2020 MK_4 (de la Fuente Marcos et al. 2021).

Figure 11 shows the result of N-body integrations backward in time for the nominal orbit and representative control orbits of 2021 UJ_5. Our results show a very chaotic dynamical past driven by frequent encounters with Jupiter and Saturn, inside the Hill radii of both planets. Our calculations suggest that its most probable source is in the Centaur population or, less likely, the trans-Neptunian region.

5 Discussion

Our statistical analyses and calculations indicate that the present-day main asteroid belt may not contain a sizeable population of minor bodies recently scattered outward by the terrestrial planets. However, it does host a non-negligible population of newcomers scattered inward by the giant planets and perhaps even captured from the Oort cloud or interstellar space. These conclusions suggest that the dynamical pathways that may have populated the early main belt may still be active today, but only in the case of material scattered inward. While asteroids from the main belt are currently scattered inward, toward the terrestrial planets (Granvik et al. 2017), the flux in the opposite direction may have ceased altogether. On the other hand, Galiazzo et al. (2016) predicted that former Centaurs and TNOs could be found in the outer asteroid belt. Our results confirm this prediction, but all the objects in Table 1 have a in the range 3.5–4.2 au.

The presence of 457175 (2008 GO_{98}) among the newcomers hints at a connection between them and the small group of active objects present in the main asteroid belt. Although the first active member of the main asteroid belt was found in 1979 (originally discovered as 1979 OW_7, rediscovered as 1996 N_2, and now known as comet 133P/Elst-Pizarro, see, for example, Jewitt et al. 2014), the nature of this population remained ambiguous. It was not until some time later that it became clear that a population of comets was present in the main asteroid belt (Hsieh and Jewitt 2006; Jewitt and Hsieh 2022). Only a very small fraction of the known members of the asteroid belt has been found to display comet-like features. Although the dominant process behind the observed cometary activity in the main belt remains unclear, possible mechanisms at work include sublimation of icy materials, impacts, rotational breakups, and electrostatic effects (see, for example, Jewitt 2012; Gundlach and Blum 2016; Gkotsinas et al. 2022). The population of main-belt comets includes several bizarre objects. The first known binary comet, 288P/(300163) 2006 VW_{139} (Agarwal et al. 2017, 2020), which is perhaps triple (Kim et al. 2020), belongs to this population that also includes a multi-tailed comet, P/2013 P5 (Jewitt et al. 2013), and objects involved in impacts and disruption events as in the cases of (596) Scheila (Jewitt et al. 2011), (6478) Gault (Moreno

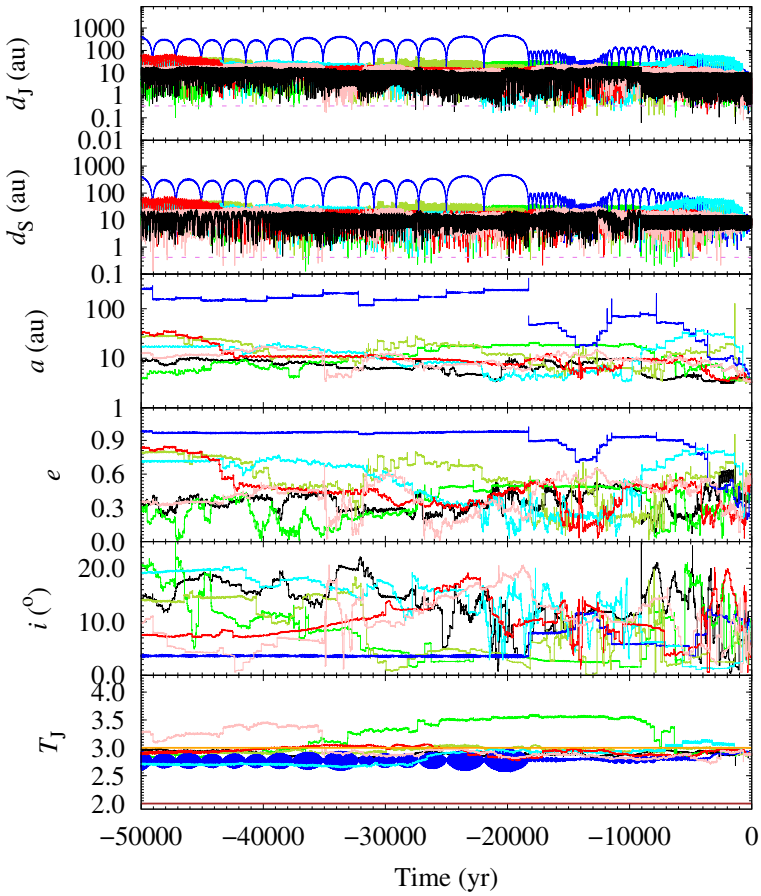

Fig. 11 Short-term past evolution of relevant parameters of 2021 UJ_5. We show the evolution of the distance to Jupiter (top panel) and Saturn (second to top) of the nominal orbit (in black) as described by the corresponding orbit determination in Table 6 of Appendix A and those of control orbits or clones with Cartesian vectors separated $+3\sigma$ (in green), -3σ (in lime), $+6\sigma$ (in blue), -6σ (in cyan), $+9\sigma$ (in red), and -9σ (in pink) from the nominal values in Table 10 of Appendix B. The Hill radii of Jupiter, 0.338 au, and Saturn, 0.412 au, are shown in red. The third to top panel shows the evolution of the semimajor axis, a. The third to bottom panel shows the evolution of the eccentricity, e. The second to bottom panel displays the inclination, i. The bottom panel shows the variations in the Tisserand's parameter, T_J (Murray and Dermott 1999), and includes the boundary references 2 (in brown) and 3 (in orange). The output time-step size is 1 yr, the origin of time is epoch 2459600.5 TDB. The source of the input data is JPL's `Horizons`

et al. 2019), P/2015 X6 (Moreno et al. 2016a), P/2016 G1 (Moreno et al. 2016b), P/2019 A4 (PANSTARRS) and P/2021 A5 (PANSTARRS) (Moreno et al. 2021) or 248370 (2005 QN_{173}) (Chandler et al. 2021; Hsieh et al. 2021). The N-body calculations presented in the previous section suggest that most newcomers, including 457175, 2011 QQ_{99}, and 2021 UJ_5, might have had an origin as debris from the 29P/Schwassmann-Wachmann 1–P/2008 CL94 (Lemmon)–P/2010 TO20 (LINEAR-Grauer) cometary complex in Centaur orbital parameter space.

The outer section of the main asteroid belt has been previously studied within the context of the chaotic motion and the Lyapunov time, T_L (the inverse of the maximum Lyapunov

exponent), which could be very short for certain objects in this region (see, for example, Murison et al. 1994; Holman and Murray 1996; Winter et al. 2010). The Lyapunov time is the characteristic timescale for the exponential divergence of initially close orbits. Focusing on the objects in Table 1 with the most reliable orbit determinations, we obtained T_L=1500 yr (1100 yr for integrations into the future) for 2003 BM_1, 500 yr (500 yr) for 2011 QQ_{99}, 500 yr (600 yr) for 2020 UO_{43}, and 450 yr (800 yr) for 2021 UJ_5. Therefore, our relevant results for real objects confirm the conclusions of the analysis in Winter et al. (2010) and lend credence to the notion that some small bodies may indeed have reached the main belt within the last few hundred years. However, they may not last long in their current orbits as their T_L are also very short for integrations into the future.

The four asteroids mentioned above have Lyapunov times as short as their chaotic transport times or diffusion times. In general, this is not the case. The statistical relationship between these two timescales is not straightforward; it has a large scatter and its fitting is approximately quadratic (see, for example, Murray and Holman 1997; Shevchenko 1998). A dramatic example of this fact is in the asteroid 522 Helga, which is both chaotic and stable, with a short Lyapunov time but infinite diffusion time (Milani and Nobili 1993). This topic has been recently revisited by Cincotta et al. (2022).

We have pointed out above that secular resonances (other than von Zeipel–Lidov–Kozai's) may bring some of these objects back and forth into the belt from beyond Jupiter. For instance, asteroids could be perturbed by secular resonances involving the values of the longitude of perihelion and the ascending node relative to those of Saturn (see, for example, Williams 1969; Froeschle and Scholl 1986, 1987, 1988, 1989; Yoshikawa 1987; Morbidelli and Henrard 1991a, b). The role of the so-called ν_6 secular resonance can be explored by studying the evolution of the resonant argument σ_6=$\varpi - \varpi_6$, where ϖ=Ω+ω is the longitude of perihelion of the asteroid and the one of Saturn is ϖ_6. According to Williams (1969), two resonant states are possible with libration of σ_6 around 0^o (when the perihelia of the asteroid and Saturn are approximately aligned) or 180^o (when the perihelia are somewhat anti-aligned), for additional details see, for example, Carruba and Morbidelli (2011) and Huaman et al. (2018). The secular nodal resonance with Saturn can be assessed by studying the resonant argument $\Omega - \Omega_6$. Using JPL's `Horizons` data, we have explored these secular resonances for 457175, 2003 BM_1, 2011 QQ_{99}, 2020 UO_{43}, and 2021 UJ_5. The secular nodal resonance does not seem to be currently active for any of these objects, but Fig. 12 shows that at least two objects are, have been, or will be subjected to the ν_6 secular resonance. Comet 362P or 457175 may have engaged in anti-aligned ν_6 secular resonant behavior in the past and 2021 UJ_5 seems to be currently trapped in the ν_6 secular resonance with σ_6 oscillating about 0^o. Figure 13 shows that librations of σ_6 are also observed for other objects, but not about 0^o or 180^o. However, and given the rather short values of T_L pointed out above, any resonant engagements are expected to be relatively brief.

Our analyses have also uncovered a possible gravitational trap in the outer main belt for interstellar objects entering the Solar system at relatively slow speeds with respect to the barycenter; in other words, objects following hyperbolic orbits with low excess eccentricity, $\sim$1 to 1.3. Asteroid 2020 UO_{43} might be one of such objects but its current orbit determination is not precise enough to confirm (or reject) an interstellar origin (see also the cautionary note above).

As pointed out in Sect. 2, we have not considered the Yarkovsky and Yarkovsky–O'Keefe–Radzievskii–Paddack (YORP) effects (see, for example, Bottke et al. 2006) in our calculations, although both effects have been confirmed to be detectable in both near-Earth and main-belt asteroid populations (see, for example, Farnocchia et al. 2013; Carruba et al. 2016, 2017; Del Vigna et al. 2018; Ďurech et al. 2018; Greenstreet et al. 2019; Greenberg

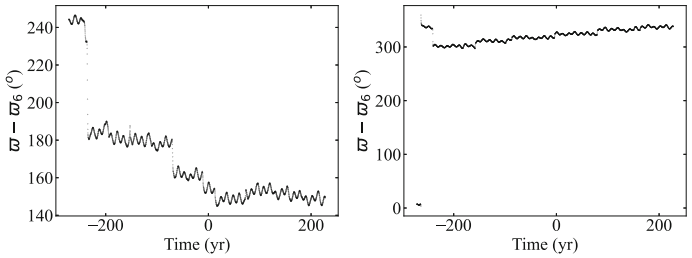

Fig. 12 Evolution of the resonant argument σ_6=$\varpi - \varpi_6$ for 457175 (2008 GO_{98}) and 2021 UJ_5, left- and right-hand side panels, respectively. The origin of time is the epoch 2459600.5 JD Barycentric Dynamical Time (2022-Jan-21.0 00:00:00.0 TDB) and the output cadence is 60 d. The source of the data is JPL's `Horizons`

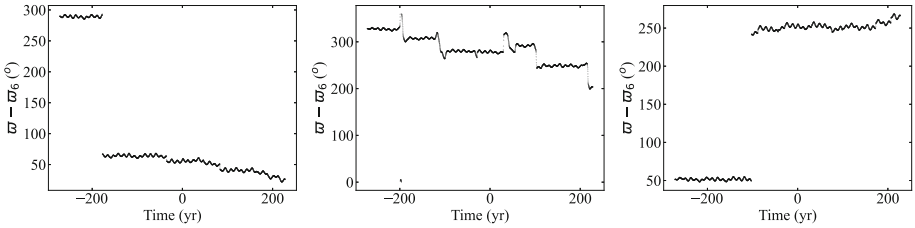

Fig. 13 Evolution of the resonant argument σ_6=$\varpi - \varpi_6$ for (from left to right) 2003 BM_1, 2011 QQ_{99}, and 2020 UO_{43}. The origin of time is the epoch 2459600.5 JD Barycentric Dynamical Time (2022-Jan-21.0 00:00:00.0 TDB) and the output cadence is 60 d. The source of the data is JPL's `Horizons`

et al. 2020). However, ignoring these effects has no significant impact on the evaluation of the short-term orbital evolution of the objects discussed here because for an average value for the Yarkovsky drift of 10^{-9} au yr^{-1} (see, for example, Nugent et al. 2012), the timescale to enter the main belt is of the order of Myr, which is several orders of magnitude longer than the time intervals discussed in this research. On the other hand, accurate modeling of the Yarkovsky force requires relatively precise knowledge of the physical properties—such as rotation rate, albedo, bulk density, surface conductivity, or emissivity—of the objects under study, which is not the case for the relevant small bodies studied in this work.

6 Conclusions

In this paper, we have discussed the details of a data mining experiment aimed at identifying present-day members of the main asteroid belt that may have reached the belt during the last few hundred years. We have used publicly available data from JPL's SBDB and `Horizons`. Our analyses show which regions of the belt are the most and the least stable and how various mean motion resonances shape the orbital architecture of the main belt. Our conclusions can be summarized as follows.

1. The inner belt and the core of the main belt do not include any known object that could be regarded as a recent arrival to the belt.
2. The outer main belt hosts a small but very interesting population of orbital newcomers. A few dozen objects may have been inserted into this region within the last few hundred years. The list of interlopers with reliable orbit determinations includes 457175 (2008 GO_{98}), 2003 BM_1, 2011 QQ_{99}, 2020 UO_{43}, and 2021 UJ_5. At least one object has

been found to exhibit cometary activity, 457175 or comet 362P, which opens an interesting connection between the interlopers singled out here and the small group of active objects present in the main asteroid belt.
3. Asteroid 2020 UO_{43} has a non-negligible probability of having an origin in the Oort cloud or even interstellar space, but its orbit determination is not sufficiently robust to reach a conclusive answer to the question of its origin, if the object is confirmed as real.
4. Most interlopers found here may come from the Centaur orbital realm.

Our results suggest that the dynamical pathways that inserted material from beyond Jupiter into the main asteroid belt early in the history of the Solar system may continue to be active today but those sending debris from the orbital realm of the terrestrial planets into the belt may be currently inactive or at least their present-day strength could be significantly weaker than that of those scattering material inward.

Acknowledgements We thank the referee, V. Carruba, for his constructive, thorough, and helpful reports, a second referee for pointing out the non-straightforward statistical relationship between Lyapunov time and diffusion time, S. J. Aarseth for providing one of the codes used in this research, A. B. Chamberlin for helping with the new JPL's Solar System Dynamics website, S. Deen for finding precovery images of some of the objects discussed here and for additional comments including the issue of the dubious linkage of 2020 UO_{43}, and A. I. Gómez de Castro for providing access to computing facilities. Part of the calculations and the data analysis were completed on the Brigit HPC server of the 'Universidad Complutense de Madrid' (UCM), and we thank S. Cano Alsúa for his help during this stage. This work was partially supported by the Spanish 'Ministerio de Economía y Competitividad' (MINECO) under grant ESP2017-87813-R and by the 'Agencia Estatal de Investigación (Ministerio de Ciencia e Innovación)' under grant PID2020-116726RB-I00 /AEI/10.13039/501100011033. In preparation for this paper, we made use of the NASA Astrophysics Data System, the ASTRO-PH e-print server, and the MPC data server.

Data Availability Statement The data underlying this paper were accessed from JPL's SBDB (https://ssd.jpl.nasa.gov/tools/sbdb_lookup.html#/) and `Horizons` on-line solar system data and ephemeris computation service (https://ssd.jpl.nasa.gov/horizons/), both provided by the Solar System Dynamics Group (https://ssd.jpl.nasa.gov/). The derived data generated in this research will be shared on reasonable request to the corresponding author.

Appendix A Orbit determinations

The orbit determinations of the objects discussed in detail in the sections are shown here (Tables 2, 3, 4, 5 and 6).

Table 2 Values of the Heliocentric Keplerian orbital elements and their respective 1σ uncertainties of 2003 BM_1

Orbital parameter		
Semimajor axis, a (au)	=	3.640089±0.000002
Eccentricity, e	=	0.5143570±0.0000010
Inclination, i (^{o})	=	11.34667±0.00003
Longitude of the ascending node, Ω (^{o})	=	350.5776±0.0002
Argument of perihelion, ω (^{o})	=	156.1809±0.0009
Mean anomaly, M (^{o})	=	247.5705±0.0002
Perihelion distance, q (au)	=	1.767783±0.000004
Aphelion distance, Q (au)	=	5.512394±0.000003
Absolute magnitude, H (mag)	=	18.2

The orbit determination is referred to epoch JD 2459600.5 (2022-Jan-21.0) TDB (Barycentric Dynamical Time, J2000.0 ecliptic and equinox), and it is based on 90 observations with a data-arc span of 5140 d (solution date, 2021-Apr-14 21:40:32 PDT). Source: JPL's SBDB

Table 3 Values of the Heliocentric Keplerian orbital elements and their respective 1σ uncertainties of 2020 UO_{43} . *Source*: JPL's SBDB

Orbital parameter		
Semimajor axis, a (au)	=	4.1360±0.0011
Eccentricity, e	=	0.64513±0.00011
Inclination, i (^{o})	=	1.7584±0.0003
Longitude of the ascending node, Ω (^{o})	=	83.552±0.009
Argument of perihelion, ω (^{o})	=	260.125±0.010
Mean anomaly, M (^{o})	=	40.38±0.02
Perihelion distance, q (au)	=	1.46775±0.00008
Aphelion distance, Q (au)	=	6.804±0.002
Absolute magnitude, H (mag)	=	19.50±0.15

The orbit determination is referred to epoch JD 2459396.5 (2021-Jul-01.0) TDB (Barycentric Dynamical Time, J2000.0 ecliptic and equinox), and it is based on 13 observations with a data-arc span of 548 d (solution date, 2021-Apr-15 23:16:16 PDT).

Table 4 Values of the Heliocentric Keplerian orbital elements and their respective 1σ uncertainties of 210718 (2000 ST_{252}). *Source*: JPL's SBDB

Orbital parameter		
Semimajor axis, a (au)	=	3.60668553±0.00000004
Eccentricity, e	=	0.39219767±0.00000003
Inclination, i (^{o})	=	7.477859±0.000005
Longitude of the ascending node, Ω (^{o})	=	74.36999±0.00005
Argument of perihelion, ω (^{o})	=	15.40597±0.00005
Mean anomaly, M (^{o})	=	342.689186±0.000010
Perihelion distance, q (au)	=	2.19215188±0.00000014
Aphelion distance, Q (au)	=	5.02121918±0.00000005
Absolute magnitude, H (mag)	=	15.18

The orbit determination is referred to epoch JD 2459600.5 (2022-Jan-21.0) TDB (Barycentric Dynamical Time, J2000.0 ecliptic and equinox), and it is based on 584 observations with a data-arc span of 7822 d (solution date, 2022-Apr-13 22:34:29 PDT)

Table 5 Values of the Heliocentric Keplerian orbital elements and their respective 1σ uncertainties of 2011 QQ_{99}. *Source*: JPL's SBDB

Orbital parameter		
Semimajor axis, a (au)	=	3.80163390±0.00000008
Eccentricity, e	=	0.4261700±0.0000003
Inclination, i (^{o})	=	3.21247±0.00003
Longitude of the ascending node, Ω (^{o})	=	1.6633±0.0003
Argument of perihelion, ω (^{o})	=	8.9432±0.0003
Mean anomaly, M (^{o})	=	134.16675±0.00004
Perihelion distance, q (au)	=	2.1814916±0.0000013
Aphelion distance, Q (au)	=	5.42177625±0.00000012
Absolute magnitude, H (mag)	=	16.5

The orbit determination is referred to epoch JD 2459600.5 (2022-Jan-21.0) TDB (Barycentric Dynamical Time, J2000.0 ecliptic and equinox), and it is based on 48 observations with a data-arc span of 8918 d (solution date, 2021-Apr-15 05:16:22 PDT).

Table 6 Values of the Heliocentric Keplerian orbital elements and their respective 1σ uncertainties of 2021 UJ_5 . *Source*: JPL's SBDB

Orbital parameter		
Semimajor axis, a (au)	=	3.3960±0.0002
Eccentricity, e	=	0.51475±0.00002
Inclination, i (^{o})	=	9.3875±0.0003
Longitude of the ascending node, Ω (^{o})	=	65.33424±0.00014
Argument of perihelion, ω (^{o})	=	351.1743±0.0012
Mean anomaly, M (^{o})	=	11.9668±0.0010
Perihelion distance, q (au)	=	1.64789±0.00002
Aphelion distance, Q (au)	=	5.1440±0.0003
Absolute magnitude, H (mag)	=	19.72

The orbit determination is referred to epoch JD 2459600.5 (2022-Jan-21.0) TDB (Barycentric Dynamical Time, J2000.0 ecliptic and equinox), and it is based on 51 observations with a data-arc span of 68 d (solution date, 2022-Jan-07 22:17:00 PST).

Appendix B Cartesian vectors

The barycentric Cartesian state vectors of the objects discussed in detail in the sections are shown here (Tables 7, 8, 9 and 10).

Table 7 Barycentric Cartesian state vector of 2003 BM_1 : components and associated 1σ uncertainties. *Source*: JPL's `Horizons`

Component		Value±1σ uncertainty
X (au)	=	$4.897320775769619\times10^{+0}\pm1.34839974\times10^{-5}$
Y (au)	=	$-5.212872303509024\times10^{-1}\pm5.05348133\times10^{-5}$
Z (au)	=	$5.752081909237879\times10^{-2}\pm1.23618711\times10^{-5}$
V_X (au/d)	=	$-1.879730452630099\times10^{-3}\pm5.60658767\times10^{-8}$
V_Y (au/d)	=	$5.817006393756842\times10^{-3}\pm3.02313450\times10^{-8}$
V_Z (au/d)	=	$1.091705108513680\times10^{-3}\pm8.31948849\times10^{-9}$

Data are referred to epoch 2459600.5, 21-January-2022 00:00:00.0 TDB (J2000.0 ecliptic and equinox).

Table 8 Barycentric Cartesian state vector of 210718 (2000 ST_{252}): components and associated 1σ uncertainties. *Source*: JPL's `Horizons`

Component		Value±1σ uncertainty
X (au)	=	$1.536584439342031\times10^{+0}\pm4.74764379\times10^{-7}$
Y (au)	=	$1.775723062487080\times10^{+0}\pm1.73163239\times10^{-7}$
Z (au)	=	$-1.324647636935953\times10^{-1}\pm2.62870805\times10^{-7}$
V_X (au/d)	=	$-1.116266081601603\times10^{-2}\pm1.48210777\times10^{-9}$
V_Y (au/d)	=	$6.472903689610230\times10^{-3}\pm9.95711599\times10^{-10}$
V_Z (au/d)	=	$1.639978110112024\times10^{-3}\pm1.30296247\times10^{-9}$

Data are referred to epoch 2459600.5, 21-January-2022 00:00:00.0 TDB (J2000.0 ecliptic and equinox).

Table 9 Barycentric Cartesian state vector of 2011 QQ_{99}: components and associated 1σ uncertainties. *Source*: JPL's `Horizons`

Component		Value$\pm 1\sigma$ uncertainty
X (au)	=	$-5.088605123745555\times10^{+0}\pm1.06554528\times10^{-6}$
Y (au)	=	$9.382269468486346\times10^{-1}\pm3.14616410\times10^{-6}$
Z (au)	=	$6.091157848659857\times10^{-2}\pm9.27918730\times10^{-7}$
V_X (au/d)	=	$-2.536954036137189\times10^{-3}\pm2.13416890\times10^{-9}$
V_Y (au/d)	=	$-5.505587343920672\times10^{-3}\pm3.72951351\times10^{-9}$
V_Z (au/d)	=	$-3.041369097484084\times10^{-4}\pm3.48439024\times10^{-9}$

Data are referred to epoch 2459600.5, 21-January-2022 00:00:00.0 TDB (J2000.0 ecliptic and equinox).

Table 10 Barycentric Cartesian state vector of 2021 UJ_5: components and associated 1σ uncertainties. *Source*: JPL's `Horizons`

Component		Value$\pm 1\sigma$ uncertainty
X (au)	=	$-2.335857504258083\times10^{-1}\pm9.68577354\times10^{-6}$
Y (au)	=	$1.780329374916908\times10^{+0}\pm3.05919872\times10^{-5}$
Z (au)	=	$1.565833140371389\times10^{-1}\pm5.84106645\times10^{-6}$
V_X (au/d)	=	$-1.529097469644606\times10^{-2}\pm4.78188519\times10^{-8}$
V_Y (au/d)	=	$1.569062550517957\times10^{-3}\pm2.26363719\times10^{-7}$
V_Z (au/d)	=	$2.405822479905948\times10^{-3}\pm9.80029822\times10^{-8}$

Data are referred to epoch 2459600.5, 21-January-2022 00:00:00.0 TDB (J2000.0 ecliptic and equinox).

Appendix C Additional new arrivals

Figure 14 shows the evolution of relevant orbital elements for the objects in Table 1 with the most uncertain orbit determinations. All of them appear to have a short-term origin in Centaur orbital parameter space and a few might be debris from the 29P/Schwassmann-Wachmann 1–P/2008 CL94 (Lemmon)–P/2010 TO20 (LINEAR-Grauer) cometary complex.

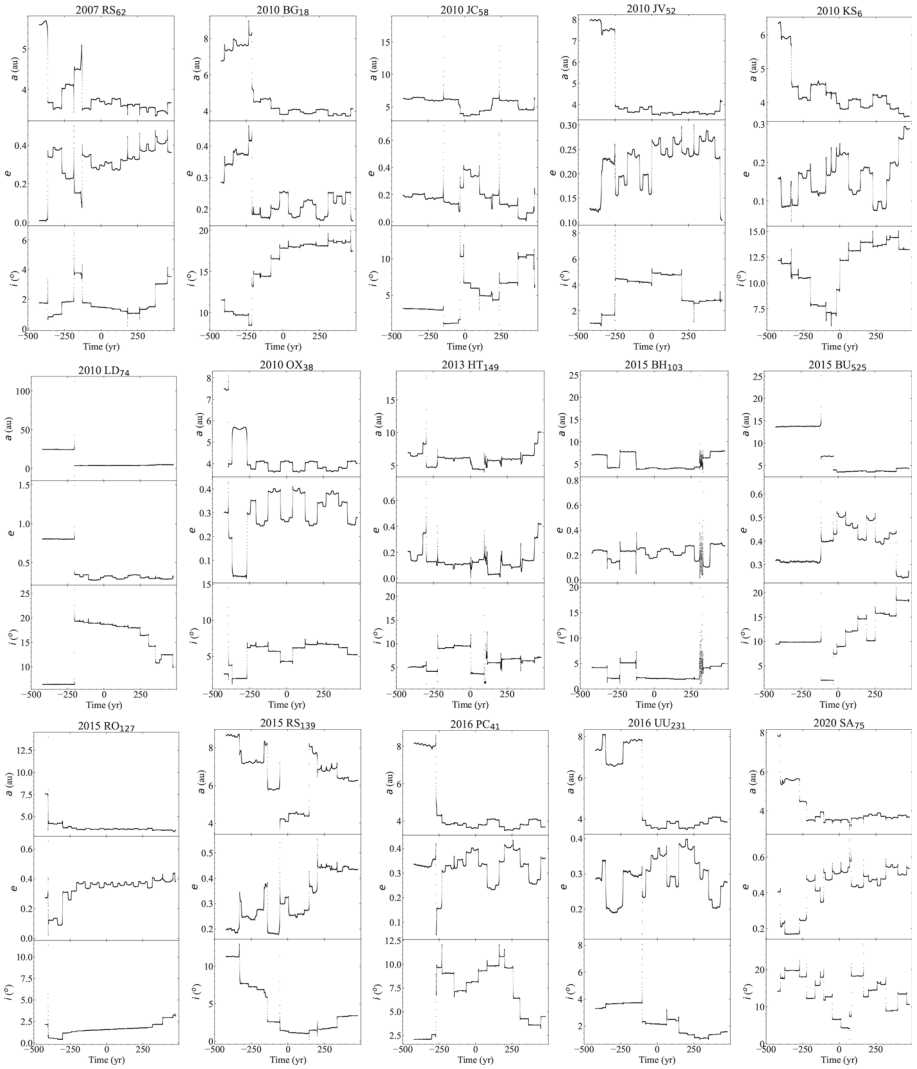

Fig. 14 Evolution of the orbital elements semimajor axis (top panels), eccentricity (middle panels), and inclination (bottom panels) for the nominal orbits of 2007 RS_{62}, 2010 BG_{18}, 2010 JC_{58}, 2010 JV_{52}, 2010 KS_6, 2010 LD_{74}, 2010 OX_{38}, 2013 HT_{149}, 2015 BH_{103}, 2015 BU_{525}, 2015 RO_{127}, 2015 RS_{139}, 2016 PC_{41}, 2016 UU_{231}, and 2020 SA_{75}. The origin of time is the epoch 2459600.5 JD Barycentric Dynamical Time (2022-Jan-21.0 00:00:00.0 TDB) and the output cadence is 30 d. The source of the data is JPL's `Horizons`

References

Aarseth, S.J.: Gravitational N-Body Simulations. Cambridge University Press, Cambridge (2003)

Agarwal, J., Jewitt, D., Mutchler, M., Weaver, H., Larson, S.: A binary main-belt comet. Nature **549**(7672), 357–359 (2017). https://doi.org/10.1038/nature23892

Agarwal, J., Kim, Y., Jewitt, D., Mutchler, M., Weaver, H., Larson, S.: Component properties and mutual orbit of binary main-belt comet 288P/(300163) 2006 VW_{139}. Astron. Astrophys. **643**, A152 (2020). https://doi.org/10.1051/0004-6361/202038195

Alfvén, H.: On the origin of the asteroids. Icarus **3**(1), 52–56 (1964). https://doi.org/10.1016/0019-1035(64)90030-2

Bailey, B.L., Malhotra, R.: Two dynamical classes of centaurs. Icarus **203**(1), 155–163 (2009). https://doi.org/10.1016/j.icarus.2009.03.044,0906.4795

Bannister, M.T., Bhandare, A., Dybczyński, P.A., Fitzsimmons, A., Oumuamua ISSI Team, et al.: The natural history of 'Oumuamua. Nat. Astron. **3**, 594–602 (2019). https://doi.org/10.1038/s41550-019-0816-x

Barucci, M.A., Brown, M.E., Emery, J.P., Merlin, F.: Composition and Surface Properties of Transneptunian Objects and Centaurs, p. 143. University of Arizona Press, Tucson (2008)

Bernardi, F.: Next challenges for the NEODyS and AstDyS data processing systems. In: IAU General Assembly, vol 29, p 2235184 (2015) https://ui.adsabs.harvard.edu/abs/2015IAUGA..2235184B/abstract

Bobrovnikoff, N.T.: The origin of asteroids. PASP **43**(255), 324 (1931). https://doi.org/10.1086/124152

Borysenko, S., Baransky, A., Musiichuk, E.: Photometric observations of ecliptic comet 47P/Ashbrook-Jackson and selected quasi-Hilda and main-belt comets at Kyiv Comet Station (MPC code-585) in 2017. Icarus **317**, 44–47 (2019). https://doi.org/10.1016/j.icarus.2018.07.003

Bottke, J., William, F., Vokrouhlický, D., Rubincam, D.P., Nesvorný, D.: The Yarkovsky and Yorp effects: implications for asteroid dynamics. Ann. Rev. Earth Planet. Sci. **34**, 157–191 (2006). https://doi.org/10.1146/annurev.earth.34.031405.125154

Brož, M., Vokrouhlický, D.: Asteroid families in the first-order resonances with Jupiter. Mon. Not. R. Astron. Soc. **390**(2), 715–732 (2008). https://doi.org/10.1111/j.1365-2966.2008.13764.x

Carruba, V., Morbidelli, A.: On the first ν_6 anti-aligned librating asteroid family of Tina. Mon. Not. R. Astron. Soc. **412**(3), 2040–2051 (2011). https://doi.org/10.1111/j.1365-2966.2010.18083.x

Carruba, V., Nesvorný, D., Aljbaae, S., Huaman, M.E.: Dynamical evolution of the Cybele asteroids. Mon. Not. R. Astron. Soc. **451**(1), 244–256 (2015). https://doi.org/10.1093/mnras/stv997

Carruba, V., Nesvorný, D., Vokrouhlický, D.: Detection of the YORP effect for small asteroids in the Karin cluster. Astron. J. **151**(6), 164 (2016). https://doi.org/10.3847/0004-6256/151/6/164

Carruba, V., Vokrouhlický, D., Nesvorný, D.: Detection of the Yarkovsky effect for C-type asteroids in the Veritas family. Mon. Not. R. Astron. Soc. **469**(4), 4400–4413 (2017). https://doi.org/10.1093/mnras/stx1186

Chamberlin, A.B., Yeomans, D.K., Chodas, P.W., Giorgini, J.D., Jacobson, R.A., Keesey, M.S., et al.: JPL solar system dynamics WWW site. In: AAS/Division for Planetary Sciences Meeting Abstracts #29, AAS/Division for Planetary Sciences Meeting Abstracts, vol 29, p 21.06 (1997) https://ui.adsabs.harvard.edu/abs/1997DPS....29.2106C/abstract

Chandler, C.O., Trujillo, C.A., Hsieh, H.H.: Recurrent activity from active asteroid (248370) 2005 QN_{173}: a main-belt comet. Astrophys. J. Lett. **922**(1), L8 (2021). https://doi.org/10.3847/2041-8213/ac365b

Chebotarev, G.A.: On the dynamical limites of the solar system. Sov. Astron. **8**, 787 (1965)

Cincotta, P.M., Giordano, C.M., Shevchenko, I.I.: Revisiting the relation between the Lyapunov time and the instability time. Phys. D Nonlinear Phenom. **430**, 133101 (2022). https://doi.org/10.1016/j.physd.2021.133101

de la Fuente Marcos, C., de la Fuente Marcos, R.: On the dynamical evolution of 2002 VE_{68}. Mon. Not. R. Astron. Soc. **427**(1), 728–739 (2012). https://doi.org/10.1111/j.1365-2966.2012.21936.x

de la Fuente Marcos, C., de la Fuente Marcos, R.: Asteroid 2015 DB_{216}: a recurring co-orbital companion to Uranus. Mon. Not. R. Astron. Soc. **453**(2), 1288–1296 (2015). https://doi.org/10.1093/mnras/stv1725

de la Fuente Marcos, C., de la Fuente Marcos, R.: Pole, pericenter, and nodes of the interstellar minor body A/2017 U1. Res. Notes Am. Astron. Soc. **1**(1), 5 (2017). https://doi.org/10.3847/2515-5172/aa96b4

de la Fuente Marcos, C., de la Fuente Marcos, R., Aarseth, S.J.: Chasing the Chelyabinsk asteroid N-body style. Astrophys. J. **812**(1), 26 (2015). https://doi.org/10.1088/0004-637X/812/1/26

de la Fuente Marcos, C., de la Fuente Marcos, R., Licandro, J., Serra-Ricart, M., Martino, S., de León, J., et al.: The active centaur 2020 MK_4. Astron. Astrophys. **649**, A85 (2021). https://doi.org/10.1051/0004-6361/202039117

de la Fuente, Marcos C., de la Fuente, Marcos R.: Erratum: pole, pericenter, and nodes of the interstellar minor body A/2017 U1. Res. Notes Am. Astron. Soc. **1**(1), 9 (2017). https://doi.org/10.3847/2515-5172/aa97d6

Del Vigna, A., Faggioli, L., Milani, A., Spoto, F., Farnocchia, D., Carry, B.: Detecting the Yarkovsky effect among near-Earth asteroids from astrometric data. Astron. Astrophys. **617**, A61 (2018). https://doi.org/10.1051/0004-6361/201833153

Di Sisto, R.P., Brunini, A.: The origin and distribution of the Centaur population. Icarus **190**(1), 224–235 (2007). https://doi.org/10.1016/j.icarus.2007.02.012

Di Sisto, R.P., Rossignoli, N.L.: Centaur and giant planet crossing populations: origin and distribution. Celest. Mech. Dyn. Astron. **132**(6–7), 36 (2020). https://doi.org/10.1007/s10569-020-09971-7

Díaz, C.G., Gil-Hutton, R.: Collisional activation of asteroids in cometary orbits. Astron. Astrophys. **487**(1), 363–367 (2008). https://doi.org/10.1051/0004-6361:20079236

Durech, J., Vokrouhlický, D., Pravec, P., Hanuš, J., Farnocchia, D., Krugly, Y.N., et al.: YORP and Yarkovsky effects in asteroids (1685) Toro, (2100) Ra-Shalom, (3103) Eger, and (161989) Cacus. Astron. Astrophys. **609**, 86 (2018). https://doi.org/10.1051/0004-6361/201731465

Farnocchia, D., Chesley, S.R., Vokrouhlický, D., Milani, A., Spoto, F., Bottke, W.F.: Near Earth asteroids with measurable Yarkovsky effect. Icarus **224**(1), 1–13 (2013). https://doi.org/10.1016/j.icarus.2013.02.004

Ferraz-Mello, S., Michtchenko, T.A., Nesvorný, D., Roig, F., Simula, A.: The depletion of the Hecuba gap vs the long-lasting Hilda group. Planet. Space Sci. **46**(11–12), 1425–1432 (1998). https://doi.org/10.1016/S0032-0633(98)00023-3

Freedman, D., Diaconis, P.: On the histogram as a density estimator:l2 theory. Zeitschrift für Wahrscheinlichkeitstheorie und Verwandte Gebiete **57**, 453–476 (1981)

Froeschle, C., Scholl, H.: The secular resonance ν_6 in the asteroidal belt. Astron. Astrophys. **166**(1–2), 326–332 (1986)

Froeschle, C., Scholl, H.: Orbital evolution of asteroids near the secular resonance ν_6. Astron. Astrophys. **179**(1–2), 294–303 (1987)

Froeschle, C., Scholl, H.: Secular resonances: new results. Celest. Mech. **43**(1–4), 113–117 (1988). https://doi.org/10.1007/BF01234558

Froeschle, C., Scholl, H.: The three principal secular resonances ν_5, ν_6, and ν_{16} in the asteroidal belt. Celest. Mech. Dyn. Astron. **46**(3), 231–251 (1989). https://doi.org/10.1007/BF00049260

Galiazzo, M.A., Wiegert, P., Aljbaae, S.: Influence of the Centaurs and TNOs on the main belt and its families. Astrophys. Space Sci. **361**(12), 371 (2016). https://doi.org/10.1007/s10509-016-2957-z

Gallardo, T.: Atlas of the mean motion resonances in the solar system. Icarus **184**(1), 29–38 (2006). https://doi.org/10.1016/j.icarus.2006.04.001

Gallardo, T.: Strength, stability and three dimensional structure of mean motion resonances in the solar system. Icarus **317**, 121–134 (2019). https://doi.org/10.1016/j.icarus.2018.07.002

García-Migani, E., Gil-Hutton, R.: The activity and dynamical evolution of quasi-hilda asteroid (457175) 2008 GO98. Planet. Space Sci. **160**, 12–18 (2018). https://doi.org/10.1016/j.pss.2018.03.011

Ginsburg, A., Sipőcz, B.M., Brasseur, C.E., Cowperthwaite, P.S., Craig, M.W., Deil, C., Guillochon, J., Guzman, G., Liedtke, S., Lian Lim, P., Lockhart, K.E., Mommert, M., Morris, B.M., Norman, H., Parikh, M., Persson, M.V., Robitaille, T.P., Segovia, J.C., Singer, L.P., Tollerud, E.J., de Val-Borro, M., Valtchanov, I., Woillez, J.: Astroquery collaboration, a subset of astropy collaboration astroquery: an astronomical web-querying package in python. Astron. J. **157**(3), 98 (2019). https://doi.org/10.3847/1538-3881/aafc33

Giorgini, J.D., Yeomans, D.K., Chamberlin, A.B., Chodas, P.W., Jacobson, R.A., Keesey, M.S., et al.: JPL's on-line solar system data service. In: AAS/Division for Planetary Sciences Meeting Abstracts #28, AAS/Division for Planetary Sciences Meeting Abstracts, vol. 28, pp. 25.04 (1996)

Giorgini, J.D., Yeomans, D.K., Chamberlin, A.B., Chodas, P.W., Jacobson, R.A., Keesey, M.S., et al.: JPL's on-line solar system ephemeris and data service. In: Bulletin of the American Astronomical Society, vol. 28, pp. 1099 (1997) https://ui.adsabs.harvard.edu/abs/1997BAAS...29.1099G/abstract

Giorgini, J.D.: Status of the JPL horizons ephemeris system. In: IAU General Assembly, vol. 29, pp. 2256293 (2015) https://ui.adsabs.harvard.edu/abs/2015IAUGA..2256293G/abstract

Giorgini, J.: Summary and status of the horizons ephemeris system. In: Capitaine N (ed) Journées Systèmes de Référence Spatio-temporels 2010, pp. 87–87 (2011)

Gkotsinas, A., Guilbert-Lepoutre, A., Raymond, S.N., Nesvorny, D.: Thermal processing of jupiter-family comets during their chaotic orbital evolution. Astrophys. J. **928**(1), 43 (2022). https://doi.org/10.3847/1538-4357/ac54ac

Granvik, M., Morbidelli, A., Vokrouhlický, D., Bottke, W.F., Nesvorný, D., Jedicke, R.: Escape of asteroids from the main belt. Astron. Astrophys. **598**, A52 (2017). https://doi.org/10.1051/0004-6361/201629252

Greenberg, A.H., Margot, J.L., Verma, A.K., Taylor, P.A., Hodge, S.E.: Yarkovsky drift detections for 247 near-earth asteroids. Astrophys. J. **159**(3), 92 (2020). https://doi.org/10.3847/1538-3881/ab62a3

Greenstreet, S., Farnocchia, D., Lister, T.: Measuring the Yarkovsky effect with Las Cumbres observatory. Icarus **321**, 564–571 (2019). https://doi.org/10.1016/j.icarus.2018.11.032

Gundlach, B., Blum, J.: Why are Jupiter-family comets active and asteroids in cometary-like orbits inactive? How hydrostatic compression leads to inactivity. Astron. Astrophys. **589**, A111 (2016). https://doi.org/10.1051/0004-6361/201527260

Hainaut, O.R., Meech, K.J., Micheli, M., Belton, M.S.J.: Rendezvous with 'Oumuamua. Messen. **173**, 13–16 (2018). https://doi.org/10.18727/0722-6691/5092

Harris, C.R., Millman, K.J., van der Walt, S.J., Gommers, R., Virtanen, P., Cournapeau, D., et al.: Array programming with NumPy. Nature **585**(7825), 357–362 (2020). https://doi.org/10.1038/s41586-020-2649-2

Hasegawa, S., Marsset, M., DeMeo, F.E., Bus, S.J., Geem, J., Ishiguro, M., et al.: Discovery of two TNO-like bodies in the asteroid belt. Astrophys. J. Lett. **916**(1), L6 (2021). https://doi.org/10.3847/2041-8213/ac0f05

Hasegawa, S., Marsset, M., DeMeo, F.E., Bus, S.J., Geem, J., Ishiguro, M., et al.: Discovery of two TNO-like bodies in the asteroid belt. Astrophys. J. Lett. **916**(1), L6 (2021). https://doi.org/10.3847/2041-8213/ac0f05

Helin, E.F., Pravdo, S.H., Rabinowitz, D.L., Lawrence, K.J.: Near-Earth asteroid tracking (NEAT) program. Ann. N. Y. Acad. Sci. **822**, 6 (1997). https://doi.org/10.1111/j.1749-6632.1997.tb48329.x

Hernandez, S., Hankey, M., Scott, J.: A data pipeline for the minor planet center. In: American Astronomical Society Meeting Abstracts #233, American Astronomical Society Meeting Abstracts, vol. 233, pp. 245.03 (2019) https://ui.adsabs.harvard.edu/abs/2019AAS...23324503H/abstract

Holman, M.J., Murray, N.W.: Chaos in high-order mean resonances in the outer asteroid belt. Astron. J. **112**, 1278 (1996). https://doi.org/10.1086/118098

Hsieh, H.H., Jewitt, D.: A population of comets in the main asteroid belt. Science **312**(5773), 561–563 (2006). https://doi.org/10.1126/science.1125150

Hsieh, H.H., Chandler, C.O., Denneau, L., Fitzsimmons, A., Erasmus, N., Kelley, M.S.P., et al.: Physical characterization of main-belt comet (248370) 2005 QN_{173}. Astrophys. J. Lett. **922**(1), L9 (2021). https://doi.org/10.3847/2041-8213/ac2c62

Huaman, M., Roig, F., Carruba, V., Domingos, R.C., Aljbaae, S.: The resonant population of asteroids in librating states of the ν_6 linear secular resonance. Mon. Not. R. Astron. Soc. **481**(2), 1707–1717 (2018). https://doi.org/10.1093/mnras/sty2381

Hunter, J.D.: Matplotlib: a 2D graphics environment. Comput. Sci. Eng. **9**(3), 90–95 (2007). https://doi.org/10.1109/MCSE.2007.55

Innanen, K., Mikkola, S., Wiegert, P.: The Earth-Moon system and the dynamical stability of the inner solar system. Astron. J. **116**(4), 2055–2057 (1998). https://doi.org/10.1086/300552

Ito, T., Ohtsuka, K.: The Lidov-Kozai oscillation and Hugo von Zeipel. Monogr. Environ. Earth Planets **7**(1), 1–113 (2019). https://doi.org/10.5047/meep.2019.00701.0001

Ito, T., Tanikawa, K.: Stability and instability of the terrestrial protoplanet system and their possible roles in the final stage of planet formation. Icarus **139**(2), 336–349 (1999). https://doi.org/10.1006/icar.1999.6112

Ito, T., Tanikawa, K.: Long-term integrations and stability of planetary orbits in our Solar system. Mon. Not. R. Astron. Soc. **336**(2), 483–500 (2002). https://doi.org/10.1046/j.1365-8711.2002.05765.x

Jewitt, D., Hsieh, H.H.: The Asteroid-Comet Continuum. arXiv e-prints arXiv:2203.01397, (2022)

Jewitt, D.: The active centaurs. Astron. J. **137**(5), 4296–4312 (2009). https://doi.org/10.1088/0004-6256/137/5/4296

Jewitt, D.: The active asteroids. Astron. J. **143**(3), 66 (2012). https://doi.org/10.1088/0004-6256/143/3/66

Jewitt, D., Weaver, H., Mutchler, M., Larson, S., Agarwal, J.: Hubble space telescope observations of main-belt comet (596) Scheila. Astrophys. J. Lett. **733**(1), L4 (2011). https://doi.org/10.1088/2041-8205/733/1/L4

Jewitt, D., Agarwal, J., Weaver, H., Mutchler, M., Larson, S.: The extraordinary multi-tailed main-belt comet P/2013 P5. Astrophys. J. Lett. **778**(1), L21 (2013). https://doi.org/10.1088/2041-8205/778/1/L21

Jewitt, D., Ishiguro, M., Weaver, H., Agarwal, J., Mutchler, M., Larson, S.: Hubble space telescope investigation of main-belt comet 133P/Elst-Pizarro. Astron. J. **147**(5), 117 (2014). https://doi.org/10.1088/0004-6256/147/5/117

Kaiser, N.: Pan-STARRS: a wide-field optical survey telescope array. In: Oschmann, J., Jacobus, M. (ed) Ground-based Telescopes, Society of Photo-Optical Instrumentation Engineers (SPIE) Conference Series, vol 5489, pp 11–22, (2004) https://doi.org/10.1117/12.552472

Kim, Y., Agarwal, J., Jewitt, D.: Evidence for active asteroid 288P being triple. In: AAS/Division for Planetary Sciences Meeting Abstracts, AAS/Division for Planetary Sciences Meeting Abstracts, vol. 52, pp. 217.01 (2020) https://ui.adsabs.harvard.edu/abs/2020DPS....5221701K/abstract

Knezevic, Z., Milani, A.: Asteroids dynamic site-AstDyS. In: IAU Joint Discussion, pp. P18 (2012) https://ui.adsabs.harvard.edu/abs/2012IAUJD...7P..18K/abstract

Kokhirova, G.I., Ivanova, O.V., Rakhmatullaeva, F.D., Baransky, A.V., Buriev, A.M.: Results of observations of dual-status object 2008 GO98 in 2017. Adv. Space Res. **67**(1), 639–647 (2021). https://doi.org/10.1016/j.asr.2020.10.014

Kozai, Y.: Secular perturbations of asteroids with high inclination and eccentricity. Astron. J. **67**, 591–598 (1962). https://doi.org/10.1086/108790

Królikowska, M., Dybczyński, P.A.: Oort spike comets with large perihelion distances. Mon. Not. R. Astron. Soc. **472**(4), 4634–4658 (2017). https://doi.org/10.1093/mnras/stx2157

Kuiper, G.P.: On the origin of asteroids. Astron. J. **55**, 164 (1950). https://doi.org/10.1086/106384

Laskar, J., Fienga, A., Gastineau, M., Manche, H.: La2010: a new orbital solution for the long-term motion of the Earth. Astron. Astrophys. **532**, A89 (2011). https://doi.org/10.1051/0004-6361/201116836
Lidov, M.L.: The evolution of orbits of artificial satellites of planets under the action of gravitational perturbations of external bodies. Planet. Space Sci. **9**(10), 719–759 (1962). https://doi.org/10.1016/0032-0633(62)90129-0
Lopez, A., Pacheco, R., Sanchez, S., Nomen, J., McGaha, J.E., Rogers, J.E., et al.: 2003 BM1. Minor Planet Electronic Circulars 2003-B29 (2003) https://ui.adsabs.harvard.edu/abs/2003MPEC....B...29L/abstract
Makino, J.: Optimal order and time-step criterion for Aarseth-type N-body integrators. Astrophys. J. **369**, 200 (1991). https://doi.org/10.1086/169751
Michel, P., Thomas, F.: The Kozai resonance for near-Earth asteroids with semimajor axes smaller than 2AU. Astron. Astrophys. **307**, 310 (1996)
Micheli, M., Farnocchia, D., Meech, K.J., Buie, M.W., Hainaut, O.R., Prialnik, D., et al.: Non-gravitational acceleration in the trajectory of 1I/2017 U1 ('Oumuamua). Nature **559**, 223–226 (2018). https://doi.org/10.1038/s41586-018-0254-4
Mikkola, S., Lehto, H.J.: Overlong simulations of the solar system dynamics with two alternating step-lengths. Celest. Mech. Dyn. Astron. **134**(2), 20 (2022). https://doi.org/10.1007/s10569-021-10058-0
Milani, A., Nobili, A.M.: Asteroid 522 Helga is chaotic and stable. Celest. Mech. Dyn. Astron. **56**(1–2), 323–324 (1993). https://doi.org/10.1007/BF00699743
Milani, A., Knežević, Z., Novaković, B., Cellino, A.: Dynamics of the Hungaria asteroids. Icarus **207**(2), 769–794 (2010). https://doi.org/10.1016/j.icarus.2009.12.022
Morbidelli, A., Henrard, J.: Secular resonances in the asteroid belt - theoretical perturbation approach and the problem of their location. Celest. Mech. Dyn. Astron. **51**(2), 131–167 (1991). https://doi.org/10.1007/BF00048606
Morbidelli, A., Henrard, J.: The main secular resonances ν_6, vs and ν_{16} in the asteroid belt. Celest. Mech. Dyn. Astron. **51**(2), 169–197 (1991). https://doi.org/10.1007/BF00048607
Moreno, F., Licandro, J., Cabrera-Lavers, A., Pozuelos, F.J.: Dust loss from activated asteroid P/2015 X6. Astrophys. J. **826**(2), 137 (2016). https://doi.org/10.3847/0004-637X/826/2/137
Moreno, F., Licandro, J., Cabrera-Lavers, A., Pozuelos, F.J.: Early evolution of disrupted asteroid P/2016 G1 (PANSTARRS). Astrophys. J. Lett. **826**(2), L22 (2016). https://doi.org/10.3847/2041-8205/826/2/L22
Moreno, F., Jehin, E., Licandro, J., Ferrais, M., Moulane, Y., Pozuelos, F.J., et al.: Dust properties of double-tailed active asteroid (6478) Gault. Astron. Astrophys. **624**, L14 (2019). https://doi.org/10.1051/0004-6361/201935526
Moreno, F., Licandro, J., Cabrera-Lavers, A., Morate, D., Guirado, D.: Dust environment of active asteroids P/2019 A4 (PANSTARRS) and P/2021 A5 (PANSTARRS). Mon. Not. R. Astron. Soc. **506**(2), 1733–1740 (2021). https://doi.org/10.1093/mnras/stab1841
Murison, M.A., Lecar, M., Franklin, F.A.: Chaotic motion in the outer asteroid belt and its relation to the age of the solar system. Astron. J. **108**, 2323 (1994). https://doi.org/10.1086/117245
Murray, C.D., Dermott, S.F.: Solar System Dynamics. Cambridge University Press, Cambridge (1999). https://doi.org/10.1017/CBO9781139174817
Murray, N., Holman, M.: Diffusive chaos in the outer asteroid belt. Astron. J. **114**, 1246–1259 (1997). https://doi.org/10.1086/118558
Napier, W.M., Dodd, R.J.: The missing planet. Nature **242**(5395), 250–251 (1973). https://doi.org/10.1038/242250b0
Napier, W.M., Dodd, R.J.: On the origin of the asteroids. Mon. Not. R. Astron. Soc. **166**, 469–490 (1974). https://doi.org/10.1093/mnras/166.2.469
Nugent, C.R., Margot, J.L., Chesley, S.R., Vokrouhlický, D.: Detection of semimajor axis drifts in 54 near-earth asteroids: new measurements of the Yarkovsky effect. Astron. J. **144**(2), 60 (2012). https://doi.org/10.1088/0004-6256/144/2/60
Ovenden, M.W.: Physical sciences: Bode's law and the missing planet. Nature **239**(5374), 508–509 (1972). https://doi.org/10.1038/239508a0
Park, R.S., Folkner, W.M., Williams, J.G., Boggs, D.H.: The JPL planetary and lunar ephemerides DE440 and DE441. Astron. J. **161**(3), 105 (2021). https://doi.org/10.3847/1538-3881/abd414
Petit, J.M., Morbidelli, A., Chambers, J.: The primordial excitation and clearing of the asteroid belt. Icarus **153**(2), 338–347 (2001). https://doi.org/10.1006/icar.2001.6702
Pravdo, S.H., Rabinowitz, D.L., Helin, E.F., Lawrence, K.J., Bambery, R.J., Clark, C.C., et al.: The Near-Earth asteroid tracking (NEAT) program: an automated system for telescope control, wide-field imaging, and object detection. Astron. J. **117**(3), 1616–1633 (1999). https://doi.org/10.1086/300769
Raymond, S.N., Nesvorny, D.: Vesta and Ceres. Insights from the Dawn Mission for the Origin of the Solar System, by Simone Marchi, Carol A. Raymond, and Christopher T., ISBN: 978-1-108-47973-8. Cam-

bridge, UK: Cambridge University Press, 2022, p. 227 https://ui.adsabs.harvard.edu/abs/2022vcid.book..227R/abstract

Raymond, S.N., Izidoro, A.: The empty primordial asteroid belt. Sci. Adv. **3**(9), e1701138 (2017). https://doi.org/10.1126/sciadv.1701138

Roberts, A.C., Muñoz-Gutiérrez, M.A.: Dynamics of small bodies in orbits between Jupiter and Saturn. Icarus **358**, 114201 (2021). https://doi.org/10.1016/j.icarus.2020.114201

Roig, F., Nesvorný, D., Ferraz-Mello, S.: Asteroids in the 2: 1 resonance with Jupiter: dynamics and size distribution. Mon. Not. R. Astron. Soc. **335**(2), 417–431 (2002). https://doi.org/10.1046/j.1365-8711.2002.05635.x

Rudenko, M.: Minor planet center data processing challenges. In: IAU General Assembly, vol. 29, pp. 2253004 (2015) https://ui.adsabs.harvard.edu/abs/2015IAUGA..2253004R/abstract

Rudenko, M.: Minor Planet Center: data processing challenges. In: Chesley, S. R., Morbidelli, A., Jedicke, R., Farnocchia, D. (eds.) Asteroids: New Observations, New Models, Cambridge University Press, Cambridge, vol. 318, pp. 265–269, (2016) https://doi.org/10.1017/S174392131500839X

Seligman, D., Laughlin, G., Batygin, K.: On the anomalous acceleration of 1I/2017 U1 'Oumuamua. Astrophys. J. Lett. **876**(2), L26 (2019). https://doi.org/10.3847/2041-8213/ab0bb5

Shevchenko, I.I.: On the recurrence and Lyapunov time scales of the motion near the chaos border. Phys. Lett. A **241**(1–2), 53–60 (1998). https://doi.org/10.1016/S0375-9601(98)00093-0

Stokes, G.H., Evans, J.B., Viggh, H.E.M., Shelly, F.C., Pearce, E.C.: Lincoln near-earth asteroid program (LINEAR). Icarus **148**(1), 21–28 (2000). https://doi.org/10.1006/icar.2000.6493

Tanikawa, K., Ito, T.: Subsystems in a stable planetary system. Publ. Astron. Soc. Jpn. **59**, 989 (2007). https://doi.org/10.1093/pasj/59.5.989

van der Walt, S., Colbert, S.C., Varoquaux, G.: The NumPy array: a structure for efficient numerical computation. Comput. Sci. Eng. **13**(2), 22–30 (2011). https://doi.org/10.1109/MCSE.2011.37

Van Rossum, G., Drake, F.L.: Python Tutorial. Centrum voor Wiskunde en Informatica Amsterdam, The Netherlands (1995)

Van Rossum, G., Drake, F.L.: Python 3 Reference Manual. CreateSpace, Scotts Valley, CA (2009)

Vinogradova, T.A.: Amplitude of the Lidov-Kozai I and e oscillations in asteroid families. Mon. Not. R. Astron. Soc. **468**(4), 4719–4724 (2017). https://doi.org/10.1093/mnras/stx743

von Zeipel, H.: Sur l'application des séries de M. Lindstedt à l'étude du mouvement des comètes périodiques. Astronomische Nachrichten **183** (22):345, (1910) https://doi.org/10.1002/asna.19091832202

Wall, J.V., Jenkins, C.R.: Practical Statistics for Astronomers. Cambridge University Press, Cambridge (2012)

Williams, J.G.: Secular Perturbations in the Solar System. PhD thesis, University of California, Los Angeles (1969)

Winter, O.C., Mourão, D.C., Giuliatti Winter, S.M.: Short Lyapunov time: a method for identifying confined chaos. Astron. Astrophys. **523**, A67 (2010). https://doi.org/10.1051/0004-6361/200912734

Wong, I., Mishra, A., Brown, M.E.: Photometry of active centaurs: colors of dormant active centaur nuclei. Astron. J. **157**(6), 225 (2019). https://doi.org/10.3847/1538-3881/ab1b22

Yoshikawa, M.: A simple analytical model for the secular resonance ν_6 in the asteroidal belt. Celest. Mech. **40**(3–4), 233–272 (1987). https://doi.org/10.1007/BF01235843